Research Square

Preprints are preliminary reports that have not undergone peer review.
They should not be considered conclusive, used to inform clinical practice,
or referenced by the media as validated information.

Atmospheric Heat Retention and Weakening Urban–Rural Thermal Contrast Driven by Surface Characteristics in the Indo-Gangetic Plains

Shahid Mirza
Institute of Science Nagpur
Rohini Lakshman Bhawar
Savitribai Phule Pune University
Sunil R Patil
phy.patil@iscnagpur.ac.in

Institute of Science Nagpur

Research Article

Keywords: SUHI, urban-rural thermal interaction, IGP, mitigation potential

Posted Date: October 23rd, 2026

DOI: https://doi.org/10.21203/rs.3.rs-10188965/v1

License: This work is licensed under a Creative Commons Attribution 4.0 International License.
Read Full License

Additional Declarations: No competing interests reported.

Atmospheric Heat Retention and Weakening Urban–Rural Thermal Contrast Driven by Surface Characteristics in the Indo-Gangetic Plains

Shahid Mirza[1], Rohini Lakshman Bhawar[2] and Sunil R. Patil[1*]

[1]Department of Physics, Institute of Science Nagpur, RT Road, Civil Lines, Nagpur, MS, India, 440001

[2]Department of Atmospheric and Space Sciences, Savitribai Phule Pune University, Ganeshkhind, Pune, MS, India, 411007

Corresponding Author: Sunil R. Patil

Email: phy.patil@iscnagpur.ac.in

ORCID: 0000-0002-2112-1867

Address: Department of Physics, Institute of Science, Nagpur MS, India - 440001

First Author: Shahid Mirza

Email: shahidmirzahere@gmail.com

ORCID: 0000-0003-2225-9761

Address: Department of Physics, Institute of Science, Nagpur MS, India - 440001

Second Author: Rohini Lakshman Bhawar

Email: rohinibhawar@gmail.com

ORCID: 0000-0002-2630-9511

Address: Department of Atmospheric and Space Sciences, Savitribai Phule Pune University, Ganeshkhind, Pune, MS, India, 411007

Abstract

Rapid urbanization, coupled with regional climatic and topographic constraints, has intensified the SUHI effect. This study employs an integrated methodological approach, utilizing Partial Least Squares (PLS) Regression, to identify and decouple the urban and atmospheric drivers influencing SUHI. The method is applied to, one of the world's most densely populated and highly environmentally constrained region, Indo-Gangetic Plains (IGP). Yearly as well as seasonal daytime and nighttime SUHI intensities are analysed for seven major cities of IGP by comparing two distinct five-year pentad windows spanning two decades (early: 2000–2004 and late: 2020–2024), alongside consecutive yearly seasonal monitoring across 2020–2024. Results reveal persistent nocturnal mean (max) SUHI dominance in the range of 2.12 °C – 2.67 °C (3.59°C – 4.61°C) in the recent pentad, exceeding daytime intensities across all cities and periods. Daytime urban–rural LST contrast has gradually narrowed, particularly during the pre-monsoon as rural moisture deficits, bare soils, and peri-urban expansion weaken daytime rural evaporative cooling. Also, pixel level seasonal SUHI assessment reveals anomalous behaviour; daytime SUHI exhibits spatial variance in Agra, Prayagraj, and Patna, whereas nighttime SUHI remains commonly positive for all cities (~95% of urban pixels). PLS regression analysis indicates that the built-up expansion is a primary year-round positive warming driver, while water bodies provide consistent daytime SUHI mitigation. Crucially, vegetation cooling is relatively weaker during the daytime but effectively reduces nighttime SUHI, and relative humidity largely plays as a mitigator except for post-monsoon daytime. We also observe that, persistent nighttime warming aligns with regional basin topography, synoptic flow channelling, and aerosol-mediated thermal retention. These findings emphasize the necessity of season- and diurnal-specific urban mitigation strategies tailored to shifting regional baselines.

Keywords: SUHI, urban-rural thermal interaction, IGP, mitigation potential

Highlights:

1. An integrated framework combines two-decade pentad comparisons with cross-validated PLS regression for SUHI drivers across seven IGP cities.
2. Nighttime SUHI remains continuously positive across > 95% of urban extents, led by Delhi, Agra, Kanpur, and Lucknow peaking at 4.0°C–5.5°C during pre-monsoon.
3. PLS models demonstrate that built-up surface consistently exacerbates warming and water bodies mitigate SUHI, whereas vegetation, relative humidity, and aerosols exhibit divergent roles and seasonally shifting impacts.
4. Degrading rural baseline moderation and persistent nighttime heat trapping underscore the urgent need for urban climate adaptation.

Introduction

Urbanization has become one of the most profound anthropogenic transformations since last few decades which is reshaping landscapes and altering natural climatic balances (Humbal et al., 2023; Roy et al., 2022). The UHI effect is a key consequence of the anthropogenic transformation, where cities exhibit higher temperatures than their rural surroundings, and is a serious concern (Stewart & Mills, 2021). The UHI phenomenon is particularly concerning for semi-arid, tropical and subtropical regions, especially where increasing population density, unplanned infrastructure, and changing land-use patterns have intensified thermal stress in cities (M. Das et al., 2025; Islam et al., 2024).

Understanding UHI drivers is essential for developing effective mitigation strategies. Broadly, the drivers can be mainly into urban surface indicators and environmental-climatic factors. Satellite data helps us track the urban indicators such as, Normalized Difference Vegetation Index (NDVI), signifies vegetation cover; Normalized Difference Built-up Index (NDBI), represents built-up area; and Normalized Difference Water Index (NDWI), denotes water bodies. High NDBI and low NDVI values generally indicate dense built-up areas with minimal vegetation, conditions known to enhance heat storage and reduce evapotranspiration (P. Singh et al., 2024). Similarly, NDWI reflects surface moisture availability, influencing cooling through latent heat flux (Bhaga et al., 2023; Taloor et al., 2021). In addition, population density and Aerosol Optical Depth (AOD) play crucial roles. Densely populated regions produce higher anthropogenic heat and the elevated aerosol levels could alter regions atmospheric radiative properties leading to heat trapping (Dangayach & Pandey, 2024; Wang et al., 2022). Collectively, these urban parameters could form a crucial framework for assessing the spatial heterogeneity of UHI.

Apart from the urban parameters, environmental parameters could also regulate the exchange of heat and moisture between the surface and atmosphere (Huang et al., 2022; Wu & Zhang, 2023). Factors such as wind speed, albedo, elevation etc. critically influence the intensity and persistence of UHI (Du et al., 2024; Liao et al., 2022). Lower wind speeds could limit the horizontal dispersion of heat and pollutants (Mishra & Mathew, 2022; Sharma et al., 2022). On the other hand, reduced rainfall and humidity could suppress the evaporative cooling and low

albedo surfaces absorb and retain the heat (Bhanage et al., 2023; Oh et al., 2023; Rath et al., 2022; Taloor et al., 2024).

In order to demonstrate the interplay of the environmental factors and the urban indicators, influencing UHI intensity, one can employ most thermally vulnerable region, exhibiting intense and persistent UHI signatures, such as the IGP (A. Das et al., 2024; Rao et al., 2021). IGP is among the world's most densely populated and rapidly urbanizing belts (Mehak Rattan, 2021). The urban regions within IGP are mainly situated along the fertile alluvial plains of the Ganga basin, which have experienced rapid expansion of built-up surfaces and a drastic decline in vegetation cover and open land (Gupta et al., 2023). The flat topography of region, limited wind circulation, and high aerosol load further contribute to thermal accumulation and reduced nocturnal cooling, intensifying the UHI effect (Dagestani et al., 2024; Jha et al., 2022; Nayak et al., 2023; Ramachandran & Rupakheti, 2022). Thus, the IGP represents a critical climatic hotspot for assessing the interplay of urban and environmental determinants influencing urban heat dynamics.

Most of the cities in the IGP have evolved organically over centuries with unplanned layouts and high-density cores (Coombe & Fung, 2022; Geetha B. Nambissan, 2021). As the rural buffers shrink due to deforestation, soil sealing, and reduced crop cover the rural–urban thermal gradient steepens, which diminishes the urban heat dissipation (Oğur, 2023). Maintaining and strengthening rural green belts around these cities thus becomes a critical strategy for moderating regional temperatures. The rural mitigation potential, driven by vegetation density, surface moisture, and evapotranspiration capacity, acts as a natural counterbalance to urban heat accumulation (Fadhil et al., 2023; Zheng et al., 2023). Therefore, evaluating the thermal interactions between urban cores and rural surroundings is key to develop an integrated urban–rural climate resilience framework.

Despite extensive research on urban thermal environments, a comprehensive understanding of how annual and seasonal SUHI dynamics evolve under coupled landscape alteration and atmospheric shifts remains critically limited, particularly across the IGP. This study addresses this gap by establishing an integrated framework that captures diurnal, seasonal, and multi-decadal SUHI shifts while explicitly accounting for evolving urban–rural thermal interactions. We apply this framework across seven major cities situated within the low-elevation alluvial basin of the IGP. By comparing two distinct five-year pentads (early: 2000–2004 vs. late: 2020–2024), this study captures multi-decadal structural shifts across IGP cities alongside consecutive annual seasonal assessments (2020–2024). Rather than relying on static baselines, our framework dynamically tracks environmental shifts within an outward 15 km masked rural reference zone (RRZ) to evaluate decadal changes in background cooling. Furthermore, by integrating cross-validated Partial Least Squares (PLS) regression, this work decouples the non-static, diurnally divergent influences of urban landscape and atmospheric drivers governing regional heat retention.

5. Methodology

This study employs multi-scale methodological framework combining satellite observations and empirical statistical modelling to evaluate SUHI dynamics across seven cities in the IGP. Period-specific urban extents and surrounding rural baselines are delineated to quantify daytime and nighttime SUHI intensities across two five-year pentad windows (early: 2000–2004 and late: 2020–2024), alongside recent consecutive years (2020–2024). In addition, last decadal transitions within the RRZ are tracked to examine changes in rural thermal moderation. Furthermore, the relative influences of urban landscape and atmospheric drivers are systematically evaluated by developing PLS regression model across pre-monsoon, winter, and post-monsoon seasons.

2.1 Study Area

The IGP zone is represented, and the seven cities are depicted in Figure 1. The IGP is a key zone for urban and industrial development, largely due to its proximity to the Ganga River. Geographically, it stretches from the semi-arid areas in the west to the eastern coastal regions, and from the Himalayan foothills in the north down to the Deccan Plateau in the south (Chatterjee et al., 2022). This diverse terrain creates a vast alluvial plain known for its fertile soil, flat landscape, and sharp seasonal temperature shifts. The region experiences a subtropical monsoon climate, with hot, dry summers (March, April and May) which is referred as pre-monsoon in this study, cool winters (December, January and February) and the season after rain (October and November) which is referred as post-monsoon (R. Singh et al., 2023; T. Singh et al., 2021). The detailed geographic, climatic and important characteristic information of all the selected cities is provided in the section S1 of the Supporting Information.

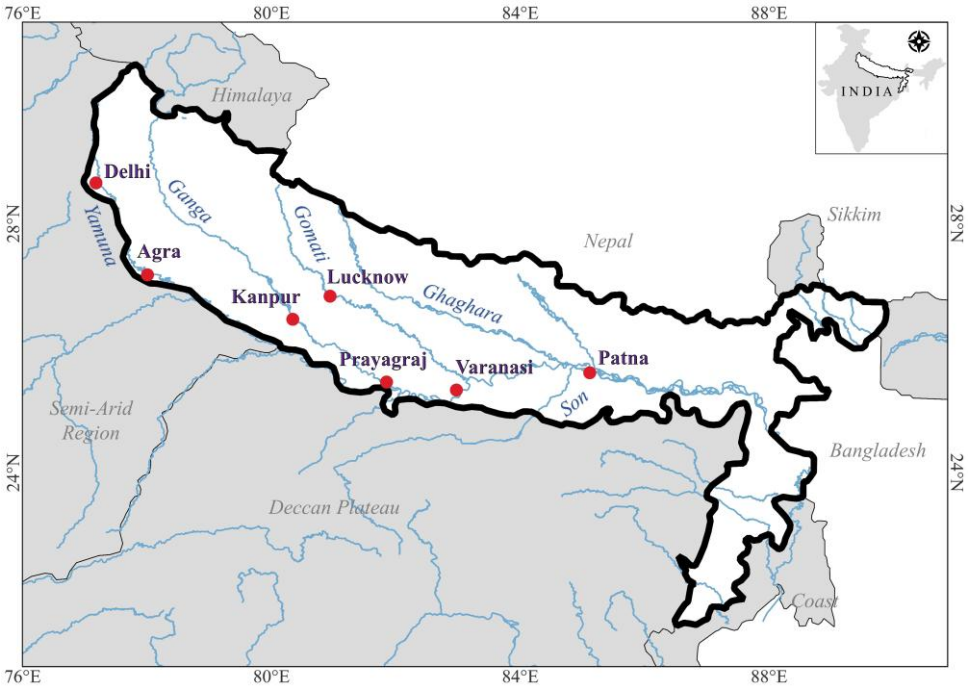


Figure 1: Geographic overview of the study area within the IGP, showing international and regional administrative boundaries; red circles designate the seven study cities, and blue lines indicate major river networks

2.2 Demarcation process of urban boundary and rural reference zone

To evaluate the spatio-temporal dynamics and to compute SUHI intensity, period-specific urban boundaries are derived dynamically for each evaluated time window. The urban boundary for each city is identified by extracting contiguous built-up surfaces via supervised classification and validating them through visual inspection in OpenSteetMap. Rather than applying a single, static boundary retrospectively, period-specific urban extents are derived to capture physical expansion dynamically: the built-up limit for the early pentad window (2000-2004) is delineated using the 2004 MODIS LULC product (MCD12Q1), while the late pentad window (2020-2024) is delineated using the corresponding 2024 LULC dataset. A visual comparison of the distinct urban extents across both windows is provided in Figure S1 of supporting information. For the surrounding baseline, previous regional and global researchers have typically delineated rural reference areas using geometric buffer zones around the urban core such as fixed buffer belts or buffers matching the urban footprint (Clinton & Gong, 2013; Debbage & Shepherd, 2015; Peng et al., 2012). Also, Recent empirical assessments have demonstrated that a buffer distance within 10–15 km captures the primary background thermal regime and landscape moderation influence relative to city scale (Yang et al., 2024). Accordingly, an outward rural reference zone (RRZ) of 15 km from the delineated urban boundary is established for each city. To overcome surface heterogeneity and avoid under or over estimation of the background temperature, all possible built-up and water body pixels within the 15 km RRZ are masked out and then called as modified RRZ (mRRZ). The remaining non-built, non-water surfaces (predominantly croplands and open vegetation) are utilized as the pure rural reference. The complete demarcation and masking workflow is illustrated in Figure 2. All spatial operations, including clipping, buffering, and masking, were conducted using QGIS 3.28 Firenze.

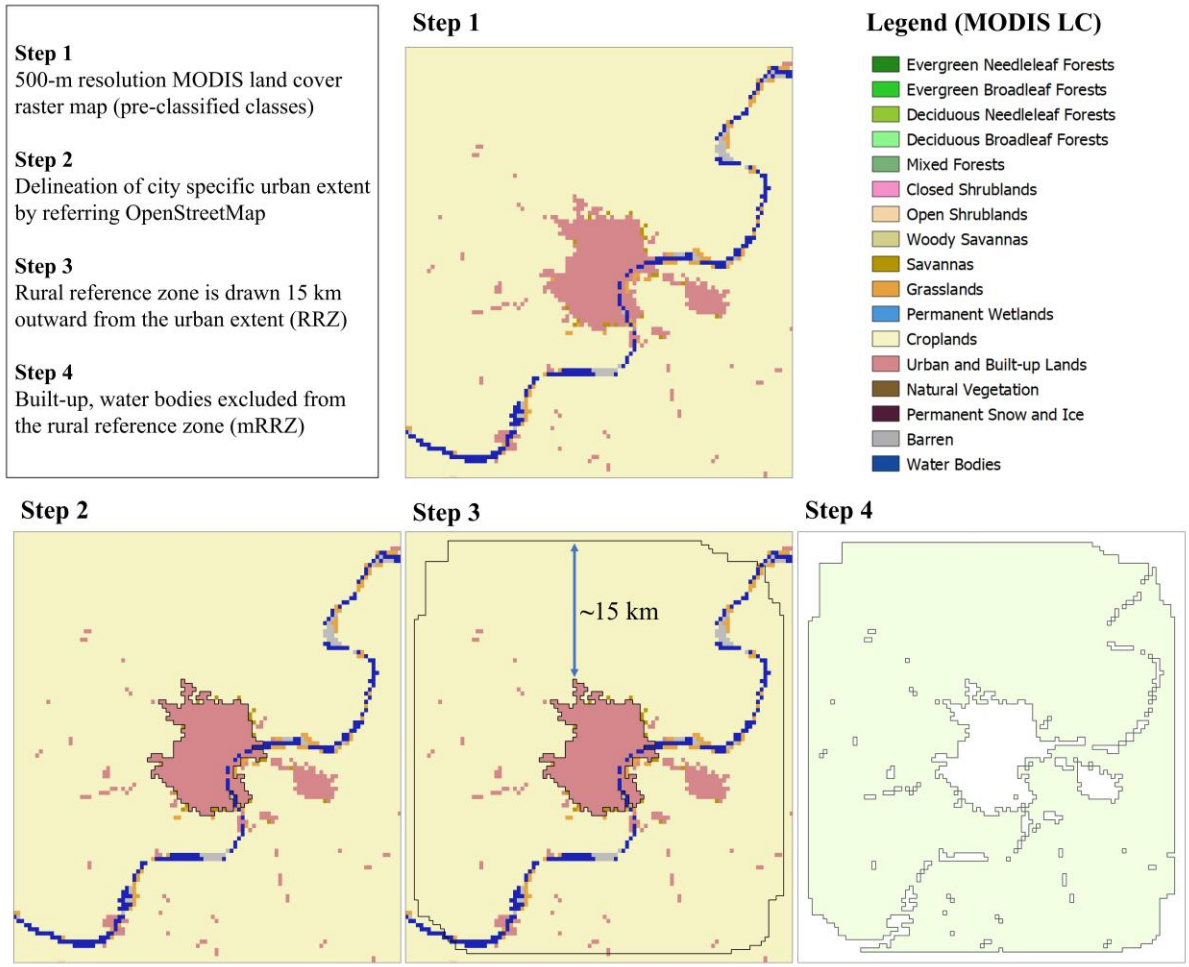


Figure 2: Methodological workflow for the delineation of urban extent, 15 km RRZ, mRRZ illustrated for Varanasi using the 2024 MODIS LULC product

2.3 SUHI intensity computation

The SUHI intensity is calculated across the delineated urban extents and their surrounding rural reference zones following the classic definition based on the direct urban-rural LST difference (Peng et al., 2012; Si et al., 2022; Yang et al., 2024; Yao et al., 2019). LST observations are obtained from the MODIS/Aqua Land Surface Temperature and Emissivity Daily L3 Global 1 km product (MYD11A1 and MYD11A2 Collection 6.1). MODIS/Aqua is selected for its equatorial overpass times of approximately 1:30 PM (local solar time) for daytime and 1:30 AM for nighttime (Wan et al., 2015). All scenes are screened using the mandatory Quality Assurance bitmasks (QC_Day and QC_Night), retaining only high-quality pixels (with cloud cover less than 5%). The raw digital numbers are calibrated to absolute thermodynamic temperature using the official scale factor ($T_K = DN \times 0.02$) and subsequently converted to degrees Celsius ($LST = T_K - 273.15$). Temporal mean composites are generated across all valid, cloud-free scenes for two pentad windows and three distinct seasons: pre-monsoon, post-monsoon, and winter.

For decadal pentad assessment, both mean (MEAN) and maximum (MAX) SUHI intensities are computed (using equation 1 and 2, respectively) for multi-year average pentad windows (early: 2000-2004 and late: 2020-2024) to assess the shifts in the SUHI pattern.

$$SUHI_{mean} = \overline{LST}_{urban} - \overline{LST}_{mRRZ} \quad (1)$$

$$SUHI_{max} = LST_{urban,max} - \overline{LST}_{mRRZ} \quad (2)$$

where $\overline{LST}_{urban}$ represents the area-weighted mean LST within the period-specific urban boundary, $LST_{urban,max}$ is the peak urban LST pixel, and $\overline{LST}_{rural}$ is the mean LST of the modified RRZ (mRRZ) which is excluding built-up lands and water bodies.

To capture seasonal variability, annual seasonal mean SUHI intensities $SUHI_{mean}$ are evaluated across individual consecutive years from 2020 to 2024.

2.4 Accessing Rural Landscape and Atmospheric Dynamics

To better understand SUHI patterns across the selected cities, multi-year variations in landscape composition and atmospheric parameters are monitored within the RRZ (15 km buffer, without modification). These dynamics are evaluated on a continuous annual basis from 2015 to 2024 to capture background environmental shifts over the recent decade. The assessment focused on empirical changes in key surface and atmospheric drivers, alongside their direct statistical relationships with rural LST and SUHI intensity.

For landscape, Vegetation Proportion (VP), Built-up and Bare Proportion (BBP), and Waterbody Proportion (WBP) are extracted using high-resolution, Sentinel-derived Dynamic World 10m near-real-time LULC dataset (Brown et al., 2022) to capture recent land-use transitions and RRZ landscape modifications. The area proportions of all three land cover classes within the RRZ are computed by equation 3.

$$P_i = \left(\frac{A_i}{A_{total}}\right) \times 100 \quad (3)$$

where P_i represents the percentage proportion of land-cover class i (e.g., vegetation, built-up and bare, or water bodies), A_i is the total area occupied by class i within the RRZ, and A_{total} is the total surface area of the delineated RRZ.

To capture atmospheric heat retention and surface moisture supported cooling, AOD and ET are considered respectively. ET represents surface moisture availability and active vegetation transpiration cooling, is acquired from the gap-filled MODIS MOD16A2GF product with 500 m spatial resolution, reported in kg/m^2/8day (Running et al., 2021) . AOD is derived from the MODIS MCD19A2 product has 1 km resolution (Lyapustin & Wang, 2022) to account for atmospheric aerosol loading and its potential role in solar radiation attenuation and nocturnal radiative trapping (Huang et al., 2022; Nikkath & Selvi, 2024).

Continuous annual relative percentage changes (%) for these parameters (VP, BBP, WBP, ET and AOD) are quantified over the recent decade. In addition, a bivariate Pearson correlation analysis is conducted to quantify the statistical association between these rural landscape-

atmospheric transitions and corresponding daytime and nighttime rural LSTs and daytime and nighttime mean SUHI intensities.

2.5 Statistical Modelling of SUHI Drivers Using PLS Regression

To identify the primary atmospheric and landscape drivers governing SUHI intensity across the IGP, PLS regression is implemented. High-dimensional landscape and atmospheric variables in urban climate studies frequently exhibit severe multicollinearity(Ding et al., 2025; Zeynali et al., 2026), resulting conventional ordinary least squares regression unstable due to variance inflation. In contrast, PLS constructs low-dimensional orthogonal latent vectors by simultaneously maximizing the covariance between explanatory variables and the response variable, retaining predictive power while overcoming collinearity(Abdi & Williams, 2010; Wold et al., 2001).

2.5.1 Predictors selection, data collection, and preprocessing

Apart from the LST data from MYD11A1 and MYD11A2 product for the SUHI analysis, other satellite datasets are used in the present study and are categorized as atmospheric and landscape parameters as represented in Table 1. The temporal scope covers three seasons such as Pre-Monsoon (March to May), Post-Monsoon (October to November), and Winter (December to February) for consecutive years from 2020 to 2024 representing the current urban development phase. All spatial datasets are brought to a common city-level support by calculating the spatial mean over the delineated urban boundaries (2024) for each seasonal window.

All the satellite datasets used in the study are atmospherically corrected as per their user manuals. All these parameters (tabulated in Table 1) are used only for the statistical models for determining their impacts on the daytime and nighttime mean SUHI intensities.

Table 1: Description of urban landscape and atmospheric predictors employed in seasonal PLS regression models

Type	Predictor	Unit	Resolution	Dataset (Satellite / Source)
Atmospheric	SNSR	MJ/m^2	~11 km (0.1°)	ERA5-Land Reanalysis
	SHF	W/m^2	~11 km (0.1°)	ERA5-Land Reanalysis
	WS	m/s	~11 km (0.1°)	ERA5-Land Reanalysis
	RH	%	~11 km (0.1°)	ERA5-Land Reanalysis
	AOD	dimensionless	1 km	MODIS (MCD19A2)
Landscape	PD	pop/km^2	100 m	WorldPop (100m/pop)
	VP	%	10 m	Sentinel-derived LC
	BBP	%	10 m	Sentinel-derived LC
	WBP	%	10 m	Sentinel-derived LC
	AL	fraction (0-1)	~11 km (0.1°)	ERA5-Land Reanalysis

Annual (season window) mean daytime and nighttime SUHI intensities are computed across the seasons using equation 1. Atmospheric parameters are acquired from the ERA5-Land reanalysis dataset (Sabater, 2019) at a spatial resolution of ~11 km. Downward surface solar radiation (SSR) and surface sensible heat flux (SHF) are derived directly from the 'surface_solar_radiation_downwards' and 'surface_sensible_heat_flux' bands, respectively. Near-surface wind speed (WS) is calculated from the orthogonal 10 m horizontal vector components ('u_component_of_wind_10m' and 'v_component_of_wind_10m') as resultant gridded wind speed.

Relative humidity (RH) is determined from 'air temperature' (T) and 'dewpoint temperature' (T_d) bands (from the ERA5-Land reanalysis dataset) via the Magnus–Tetens formulation (Lawrence, 2004). RH is defined as the ratio of actual vapor pressure 'e' to the saturation vapor pressure 'e_s' over a plane water surface at a given temperature (Alduchov et al., 1996), typically expressed as a percentage. AOD for urban extents are derived from the same MODIS MAIAC Level-2 product utilized in the rural landscape assessment.

In terms of the landscape parameters, PD (Population Density) data is extracted from the high-resolution gridded WorldPop repository (Gaughan et al., 2013; WorldPop, 2026). To align strictly with the satellite-delineated urban extents, total population is extracted within each city polygon for 2000 and 2020. A 20-year compound annual growth rate is computed to project annual population counts and density (persons/km^2) continuously for 2020–2024. Detail mathematical flow can be seen in supporting information. Detailed mathematical method for estimating WS, RH, and PD is illustrated in section S3 of supporting information.

Land cover proportions (VP, BBP, and WBP) are extracted within the delineated urban extents from high-resolution 10 m land-cover data, following the same surface area percentage formulation defined in Equation 3. Surface Albedo (AL) is acquired from the ERA5-Land hourly reanalysis dataset using the 'forecast_albedo' band, representing broadband surface reflectance.

2.5.2 PLS regression model setup

Prior to model calibration, bivariate relationships and collinearity structures across predictors are systematically evaluated using Pearson's correlation analysis (section S5 of supporting information) and Variance Inflation Factor (VIF) diagnostics (Figure 3).

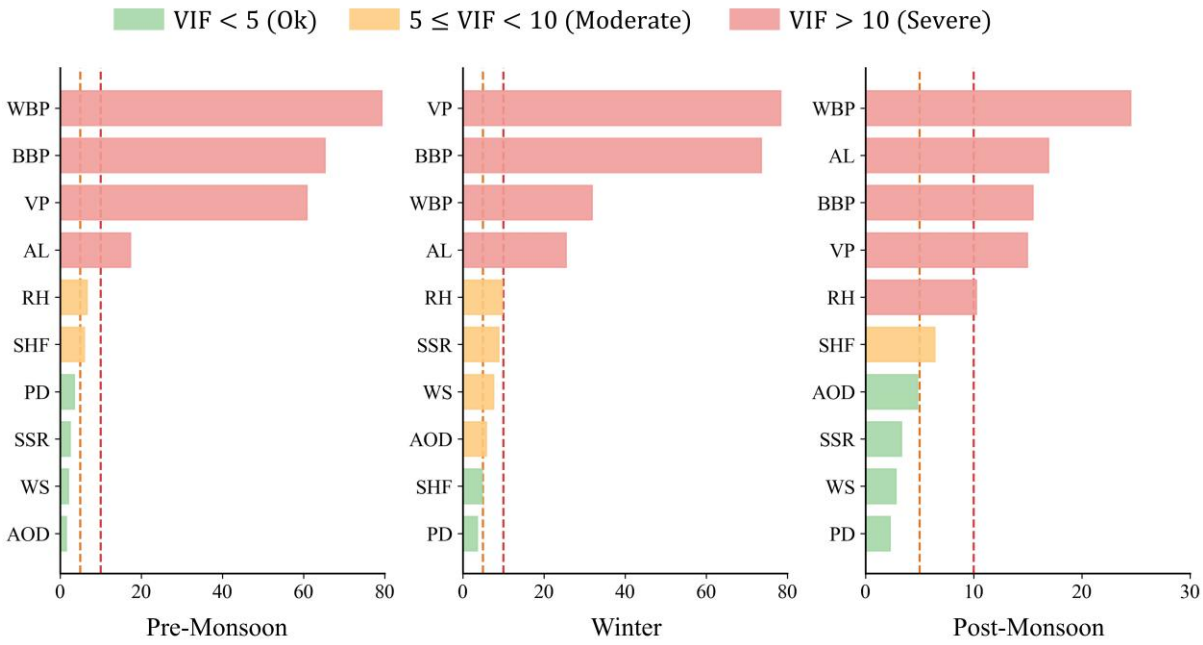


Figure 3: Seasonal multicollinearity checks for landscape and atmospheric predictors

In this study, the annual seasonal mean SUHI intensity serves as the single dependent variable (Y), while 10 atmospheric and landscape parameters serve as explanatory predictors (X) mentioned in Table 1. The models are fitted independently across distinct seasonal regimes (pre-monsoon, winter, and post-monsoon) for daytime and nighttime conditions to evaluate temporal shifts in driver dynamics. The dataset for each seasonal condition comprises N = 35 (7 cities x 5 years) annual city-level observations. Before model training, all predictor and response variables are converted to standard scores (z-score standardization, mean = 0, standard deviation = 1) to eliminate dimensional scale discrepancies.

The PLS regression model is implemented using the Non-Linear Iterative Partial Least Squares (NIPALS) algorithm for single-response systems (PLS1) via the 'scikit-learn' framework in Python(Pedregosa et al., 2018; Wold et al., 2001). In this framework, the objective is to model the linear relationship between the high-dimensional predictor space of atmospheric and landscape features and the univariate target vector of SUHI intensity. At each iteration, the algorithm calculates loading weights that maximize the sample covariance between predictor scores and response scores, capturing the dominant modes of explanatory variance directly relevant to SUHI magnitude. The number of latent components is selected independently for each model based on the maximum cross-validated Q^2 obtained from the 5-fold cross-validation procedure, partitioning the 35 observations into five balanced folds (n = 7 observations per fold). Model performance is evaluated via both the coefficient of determination of calibration (R^2) on the training set and the cross-validated predictive coefficient (Q^2) derived from out-of-fold predictions. Predictor significance is evaluated using 1000 non-parametric bootstrap resamples. Evidence of association is classified using bootstrap confidence intervals at 80% ($p < 0.20$), 90% ($p < 0.10$), and 95% ($p < 0.05$) confidence levels.

6. Results

This section presents the spatio-temporal variations in daytime and nighttime SUHI intensities comparing decadal pentad windows (2000–2004 vs. 2020–2024) and recent consecutive seasonal years (2020–2024). Observed shifts in rural baseline conditions and their influence on urban thermal contrast are evaluated. Finally, the primary landscape and atmospheric drivers governing seasonal SUHI intensities are identified.

3.1 Daytime and Nighttime SUHI Intensity Dynamics

The mean and maximum diurnal SUHI intensities for the seven IGP cities (Delhi, Agra, Kanpur, Lucknow, Prayagraj, Varanasi, and Patna) across the two pentad periods (2000–2004 and 2020–2024) are presented in Figure 4. During the daytime, mean SUHI intensities in the initial period (2000–2004) ranged from 0.03°C in Patna to 1.94°C in Lucknow. In the recent period (2020–2024), daytime mean intensities ranged between 0.36°C (Agra) and 2.42°C (Lucknow). Across the two periods, daytime mean SUHI increased in Lucknow (from 1.94°C to 2.42°C), Kanpur (from 1.30°C to 1.52°C), Varanasi (from 0.79°C to 1.30°C), and Patna (from 0.03°C to 0.56°C), while slight decreases occurred in Delhi (from 0.63°C to 0.62°C), Agra (from 0.48°C to 0.36°C), and Prayagraj (from 0.64°C to 0.56°C). Maximum daytime SUHI intensities increased in six of the seven cities, with Delhi recording the highest peak values in both 2000–2004 (3.95°C) and 2020–2024 (4.38°C), followed closely by Lucknow (increasing from 3.55°C to 4.33°C) and Patna (increasing from 2.24°C to 3.94°C). Prayagraj was the only city exhibiting a minor decline in daytime maximum SUHI, moving from 2.83°C to 2.82°C.

At nighttime, mean SUHI intensities consistently exceeded their corresponding daytime means across all cities and periods. For 2000–2004, nighttime mean SUHI ranged from 1.38°C in Patna to 2.20°C in Delhi. In 2020–2024, nighttime mean SUHI increased across all seven cities, spanning from 2.12°C in Prayagraj to 2.67°C in Delhi. Notable gains in nighttime mean SUHI are observed in Patna (from 1.38°C to 2.29°C), Varanasi (from 1.66°C to 2.37°C), and Lucknow (from 1.96°C to 2.62°C). Maximum nighttime SUHI intensities remained elevated across all cities (ranging from 3.06°C to 4.79°C in 2000–2004, and from 3.59°C to 4.61°C in 2020–2024). While Delhi and Agra showed slight reductions in nighttime maximum SUHI (from 4.79°C to 4.61°C and from 3.86°C to 3.82°C, respectively), Kanpur, Lucknow, Prayagraj, Varanasi, and Patna all exhibited increases in maximum nighttime values between the two pentads.

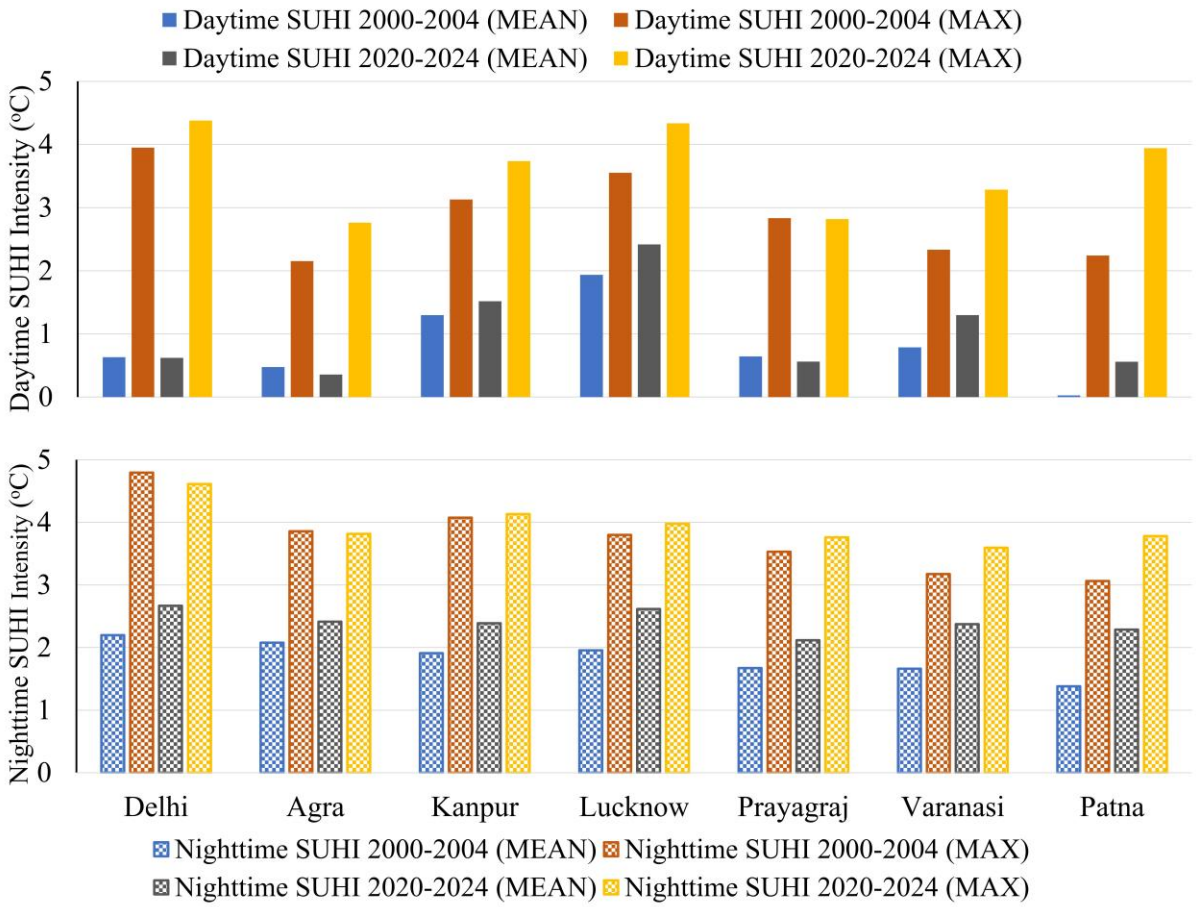
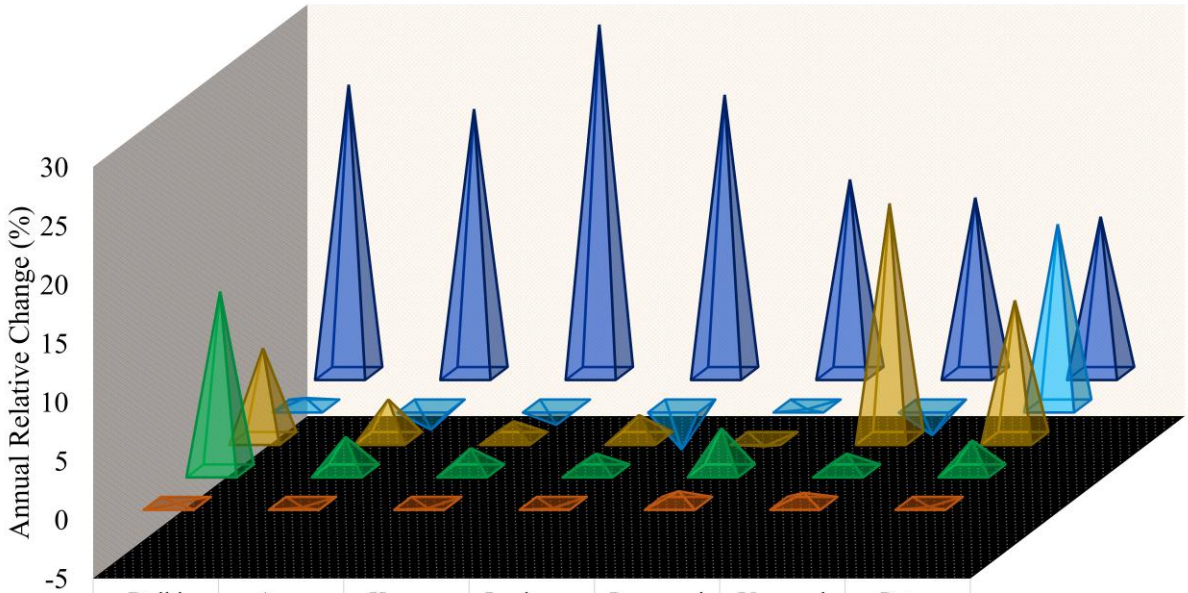


Figure 4: Comparison of mean and maximum SUHI intensities (°C) across the seven study cities for the 2000–2004 and 2020–2024 pentad windows; upper panel: daytime SUHI; lower panel: nighttime SUHI

3.2 Landscape alteration and atmospheric shifts in rural reference zone

The annual relative changes in landscape (VP, BBP, and WBP) and atmospheric (AOD and ET) parameters within the 15 km RRZ of each city evaluated over the recent decade (2015 to 2024) are presented in Figure 5. In addition, their Pearson correlations with daytime and nighttime rural LST (i.e. D-LST_r and N-LST_r) and SUHI intensity (i.e. D-SUHI and N-SUHI) are illustrated in Figure 6.



	Delhi	Agra	Kanpur	Lucknow	Prayagraj	Varanasi	Patna
AOD	0.05	-0.33	-0.40	-0.40	1.04	0.90	-0.29
VP	15.28	2.91	1.94	1.48	3.63	1.48	2.60
BBP	7.69	3.32	1.47	1.99	-0.66	20.02	11.76
WBP	0.69	-2.00	-1.60	-3.69	-0.28	-2.47	15.49
ET	24.59	22.52	29.70	23.73	16.53	14.98	13.35

Figure 5: Annual relative changes (%) in landscape and atmospheric parameters within the 15 km RRZ of each study city (2015–2024)

VP is increased across all rural peripheries, with the highest relative gain recorded in Delhi (+15.28%), while the remaining cities grew between +1.48% and +3.63%. VP demonstrated strong associations with rural thermal regimes such that is correlated negatively with nighttime rural LST ($r = -0.60$), but correlated positively with daytime rural LST ($r = 0.44$) and nighttime SUHI ($r = 0.52$). These correlations indicate contrasting diurnal relationships, where rural vegetation growth is associated with reduced nighttime LST. BBP experienced positive annual relative growth across six rural zones, headed by Varanasi (+20.02%), Patna (+11.76%), and Delhi (+7.69%), while Agra (+3.32%), Lucknow (+1.99%), and Kanpur (+1.47%) showed modest gains, and Prayagraj exhibited a minor contraction (−0.66%). In the correlation matrix, BBP correlated positively with nighttime rural LST ($r = 0.27$) and WBP ($r = 0.32$), though its correlations with SUHI intensities remained non-significant. WBP expanded noticeably in Patna (+15.49%) and slightly in Delhi (+0.69%), whereas contractions occurred across Lucknow (−3.69%), Varanasi (−2.47%), Agra (−2.00%), Kanpur (−1.60%), and Prayagraj (−0.28%). WBP is inversely correlated with daytime rural LST ($r = -0.40$), daytime SUHI ($r = -0.35$), and nighttime SUHI ($r = -0.58$).

Evapotranspiration exhibited the highest positive annual relative increase across all city peripheries, led by Kanpur (+29.70%), Delhi (+24.59%), Lucknow (+23.73%), and Agra (+22.52%), with moderate increases in Prayagraj (+16.53%), Varanasi (+14.98%), and Patna (+13.35%). ET showed a positive correlation with BBP ($r = 0.42$) and WBP ($r = 0.35$). Although displaying a weak negative association with nighttime rural LST ($r = -0.18$), its relationship was negligible during the daytime ($r = -0.02$). Annual relative changes in AOD are modest,

ranging between −0.40% (Kanpur and Lucknow) and +1.04% (Prayagraj). AOD is correlated positively with nighttime rural LST (r = 0.46) and WBP (r = 0.54), but showed significant negative correlations with nighttime SUHI (r = −0.48).

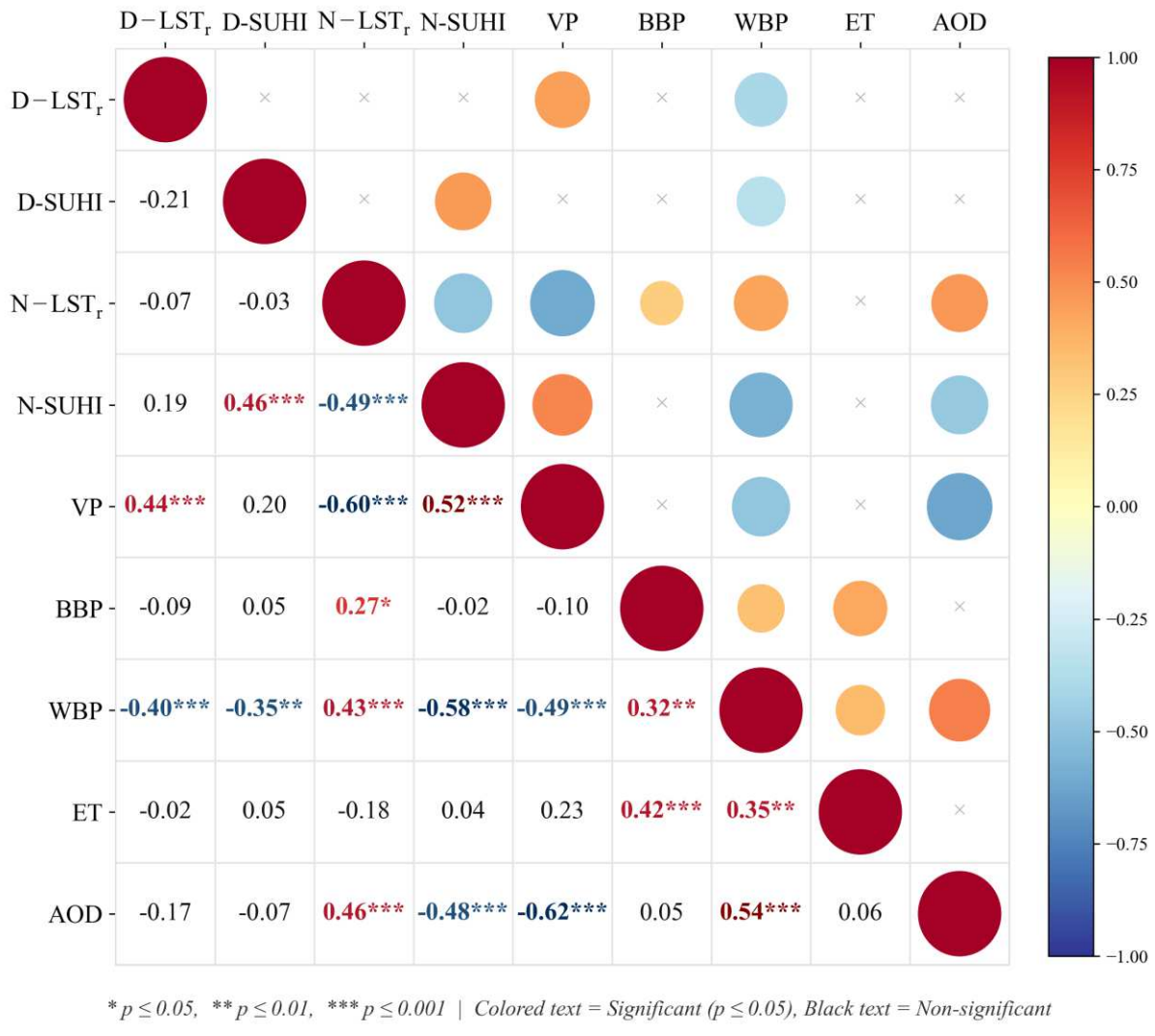


Figure 6: Pearson correlation matrix between daytime and nighttime SUHI intensities, rural baseline LST, and RRZ landscape and atmospheric parameters (2015–2024)

3.3 Seasonal variability of LST and SUHI intensity

The composite spatial distributions of daytime and nighttime LST, including both urban and RRZ for all cities, are shown in Figure 7. The maps represent mean LST for the period 2020–2024 across the pre-monsoon, winter and post-monsoon seasons. For each city, the black polygon delineates the urban boundary, while the surrounding area represents a 15 km RRZ, enabling assessment of rural-urban-rural thermal contrasts. The cities during pre-monsoon season exhibit higher day-time LSTs; 35.07°C for Delhi, 37.32°C for Agra, 36.51°C for Kanpur, 35.75°C for Lucknow, 36.61°C for Prayagraj and 36.02°C for Varanasi. Note that the daytime LST distribution in urban and rural parts appear similar as the rural-urban boundaries are increasingly being merged. However, in the nighttime we see a pronounced pre-monsoon

396 warming in the urban cores as compared to their rural counterparts. In winter, LST ranges
397 between 20.77°C and 22.97°C (12.63°C and 15.29°C) for daytime (nighttime). Post-monsoon
398 daytime LSTs show an intermediate thermal regime between pre-monsoon and winter.
399 Monsoon withdrawal leads to moderate rise in post-monsoon daytime LST, whereas the
400 nighttime LSTs significantly increases. Although the urban to rural shift is not as obvious as
401 that of pre-monsoon but it is noticeable. Urban areas continue to exhibit higher LSTs than the
402 rural (27.95°C – 29.37°C for day-time and 19.34°C – 21.93°C for night-time). In the nighttime,
403 consistent across all the cities, a gradual outward LST decay from urban centres into
404 surrounding ladders, is observed.

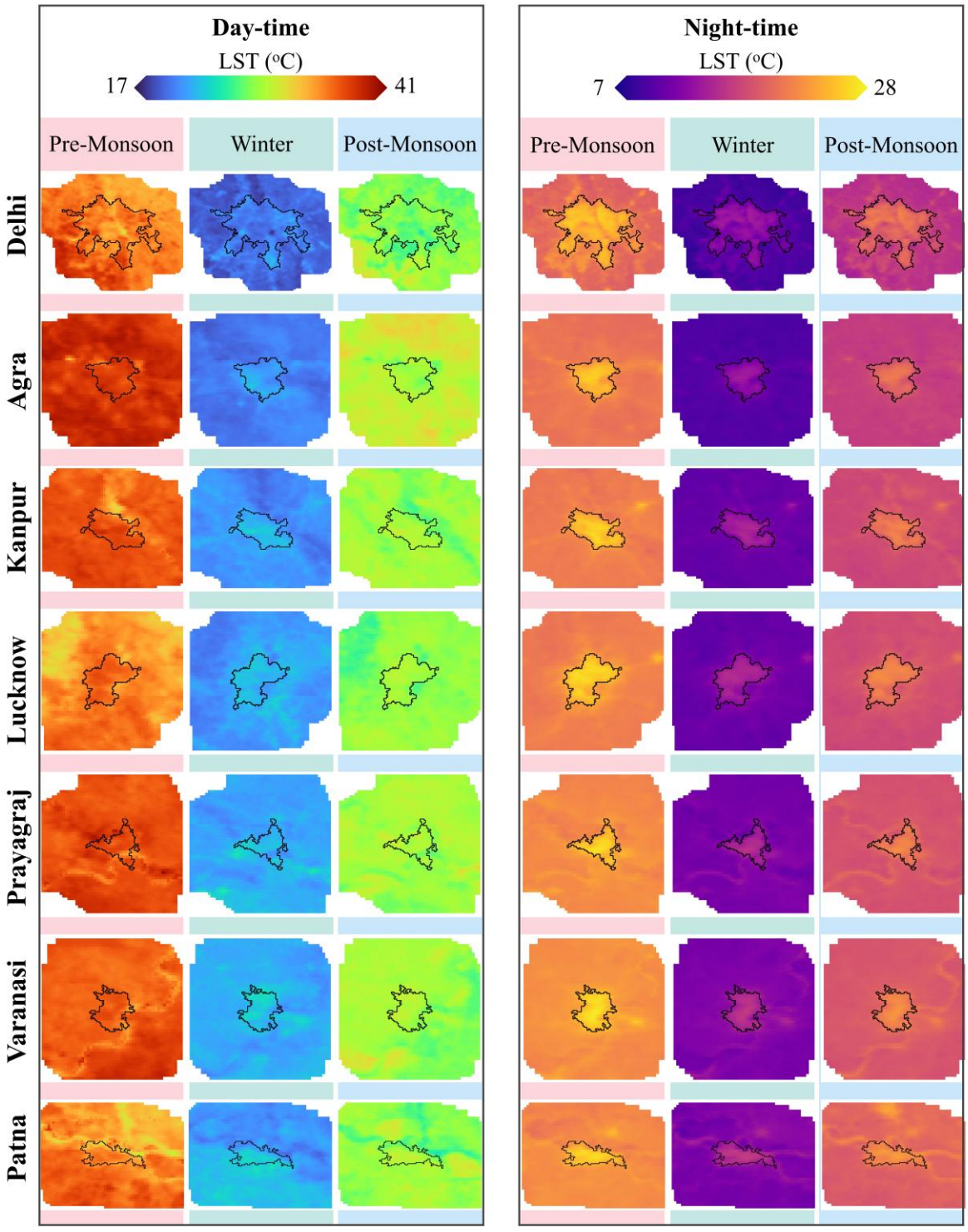


Figure 7: Spatial distribution of mean seasonal daytime and nighttime LST (°C) across the seven IGP cities and their 15 km RRZ during 2020–2024; black polygons denote the delineated urban boundaries

The pixel-level distribution and density of seasonal SUHI intensities (Figure S2) within each city are presented using violin plots in Figure 8. Daytime SUHI exhibited substantial seasonal shifts and intra-urban variance. During the pre-monsoon season, daytime SUHI distributions spanned both positive and negative values in several cities. Lucknow exhibited the most

consistently positive daytime profile, with approximately 90% of its urban pixels exceeding 0°C (peaking at 3.8°C). Kanpur and Delhi displayed broad distributions, with over 60–70% of pixels recording positive SUHI intensities, whereas in Agra, Prayagraj, Varanasi, and Patna, a substantial proportion (approximately 40–55%) of urban pixels fell at or below 0°C. In winter, daytime SUHI intensities shifted distinctly upward across all seven cities, more than 85–95% of pixels exhibited positive intensities, with distributions concentrating between 1.5°C and 4.5°C. In the post-monsoon season, daytime SUHI distributions are intermediate, with Agra exhibiting a predominantly negative regime (over 85% of pixels below 0°C, centering near −1.0°C), while Kanpur, Lucknow, Prayagraj, and Varanasi retained predominantly positive daytime intensities (60–85% of pixels above 0°C).

At nighttime, SUHI intensities remained consistently positive across virtually the entire urban extent for all cities and seasons. Over 95% of urban pixels across all seven cities maintained nighttime SUHI values above 0°C across pre-monsoon, winter, and post-monsoon. During the pre-monsoon night, pixel distributions peaked at the highest intensities, with the majority of values concentrating between 2.0°C and 5.0°C across Delhi, Agra, Kanpur, and Lucknow, and reaching upper limits near 5.5°C. Winter nighttime SUHI distributions remained elevated, with pixel densities clustered predominantly between 1.5°C and 4.0°C. In the post-monsoon season, nighttime SUHI exhibited a tight distribution centered between 1.5°C and 3.5°C across all cities, confirming sustained, positive nocturnal urban–rural thermal contrast throughout the annual cycle.

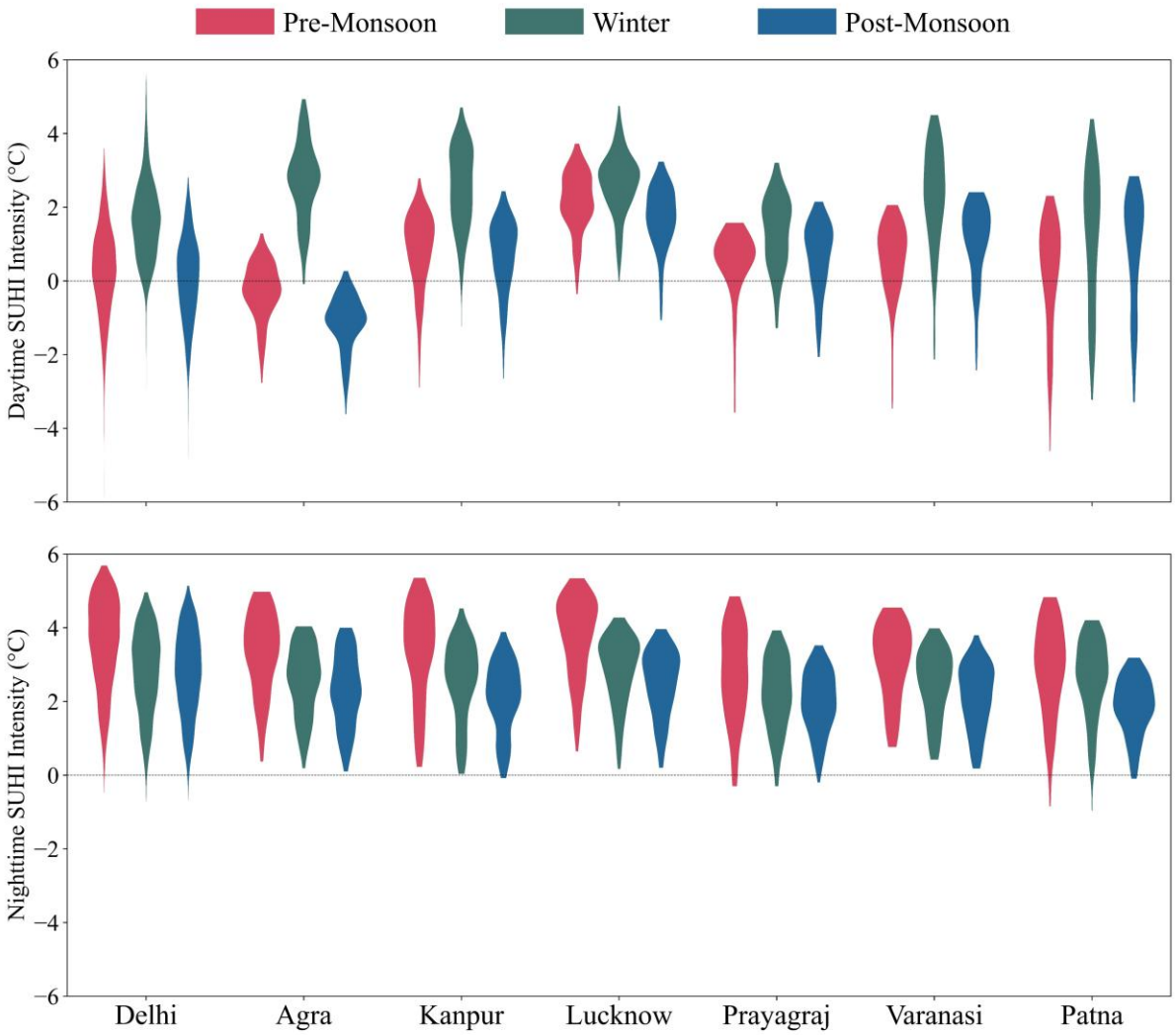


Figure 8: Pixel-level frequency distributions of seasonal daytime and nighttime SUHI intensities (°C) across the study cities (2020–2024)

3.4 Atmospheric and Landscape Drivers of Seasonal SUHI

The seasonal influences of five atmospheric (SSR, SHF, WS, AOD, and RH) alongside five landscape (PD, VP, BBP, WBP, and AL) parameters on daytime and nighttime SUHI intensities are evaluated using PLS regression (Figure 9). Standardized regression coefficients demonstrated distinct seasonal sensitivities and contrasting behavioural patterns between the built environment and atmospheric circulation regimes. The corresponding predictive performance of the calibrated and 5-fold cross-validated models across each season is also illustrated in Figure 10.

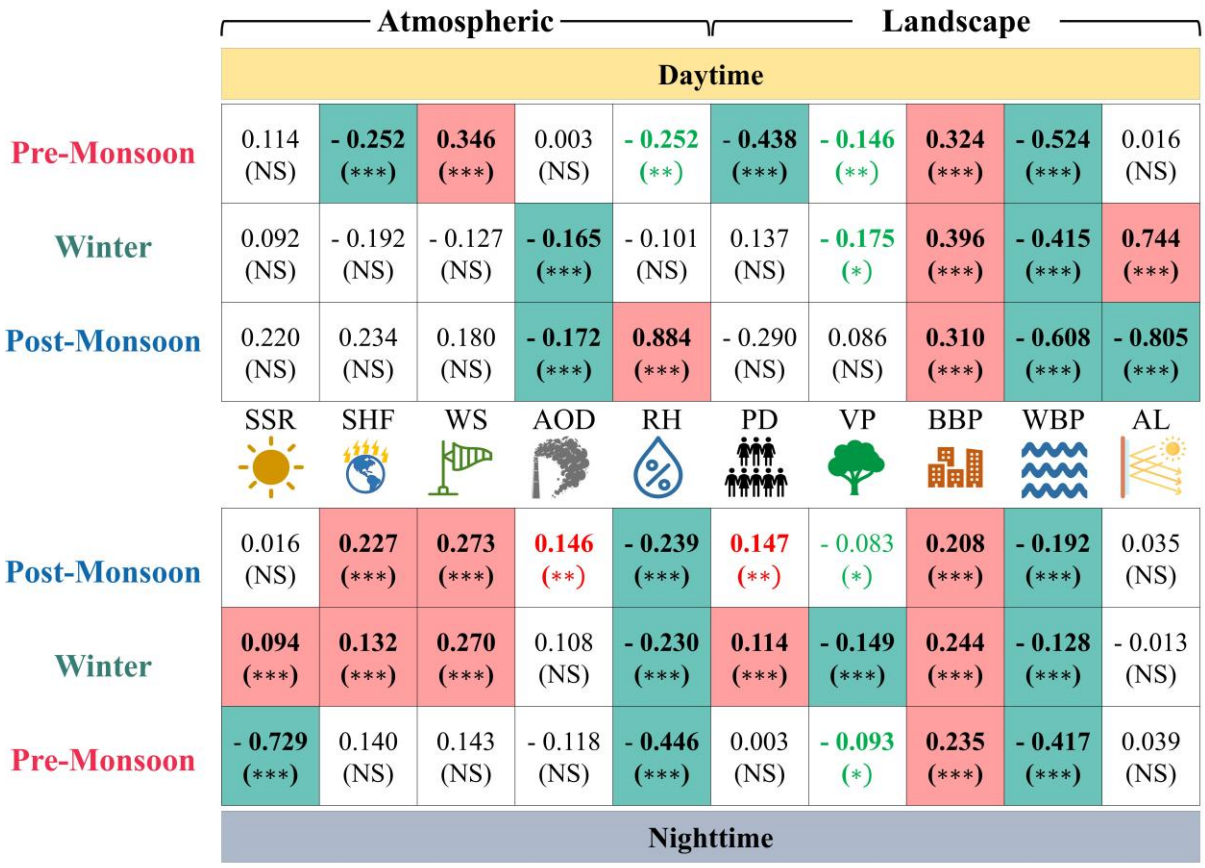


*Figure 9: Relative contributions of atmospheric and landscape predictors to seasonal daytime and nighttime SUHI intensities derived from PLS regression; colour shading indicates positive (red) and negative (green) coefficients; statistical significance thresholds are designated by asterisks (*** $p \leq 0.05$, ** $p \leq 0.1$, * $p \leq 0.2$, NS: not significant)*

During daytime, BBP served as the primary positive driver, significantly intensifying SUHI across all three seasons. In contrast, WBP consistently functioned as the strongest daytime mitigating landscape feature, maintaining significant negative coefficients throughout the pre-monsoon, winter, and post-monsoon. VP demonstrated moderate, marginal cooling tendencies during the pre-monsoon and winter seasons, whereas its daytime relationship became statistically non-significant following the monsoon withdrawal. AL exhibited pronounced seasonal reversals, exerting a strong positive influence on SUHI during winter, transitioning to an effective mitigating factor in the post-monsoon period, and remaining non-significant in the pre-monsoon. PD only reached statistical significance during the pre-monsoon daytime, displaying an inverse relationship with thermal intensity. Among the daytime atmospheric parameters, SSR remained non-significant across all seasons. Meanwhile, SHF showed a significant mitigating role restricted to the pre-monsoon, WS exacerbated heating exclusively during pre-monsoon, and AOD contributed to SUHI reduction during winter and post-monsoon. RH transitioned from a marginal cooling factor in pre-monsoon to a strong positive contributor in the post-monsoon season.

At nighttime, the enhancing role of BBP persisted as the dominant landscape driver, retaining significant positive coefficients across every season. WBP similarly sustained its mitigating

role throughout the nocturnal cycle, though its cooling magnitude is less pronounced compared to the daytime. Unlike the daytime observations, VP exhibited a consistently negative nighttime association across all seasons, with strongest statistical evidence during winter. Simultaneously, PD shifted from its daytime pattern to exert a significant positive influence on nighttime SUHI during both winter and post-monsoon periods. Nighttime atmospheric drivers exhibited strong seasonal dependency; RH served as a consistent mitigating parameter, displaying significant negative coefficients across all three seasons. Conversely, WS and SHF reinforced nighttime urban warming during winter and post-monsoon, whereas both remained non-significant in the pre-monsoon period. SSR displayed an inverse association during pre-monsoon nights and a slight warming effect in winter, while nighttime AL remained entirely non-significant across the seasons.

Scatter distributions of observed versus predicted SUHI intensities demonstrate good overall goodness-of-fit for the seasonal PLS regressions (Figure 10). Pre-monsoon models achieved the highest overall reliability, with daytime calibration and cross-validation statistics reaching $R^2 = 0.84$ (RMSEC = 0.25) and $R^2 = 0.73$ (RMSECV = 0.32), reflected by nighttime values of $R^2 = 0.83$ and $R^2 = 0.70$ (RMSECV = 0.26). Winter models maintained similarly strong predictive power across both daytime and nighttime, with cross-validated Q^2 values of 0.62 (RMSECV = 0.40) for daytime and 0.64 (RMSECV = 0.20) for nighttime. In the post-monsoon season, daytime predictive capacity declined noticeably (cross-validated $Q^2 = 0.30$, RMSECV = 0.72), whereas nighttime performance recovered robust explanatory strength ($Q^2 = 0.74$, cross-validated $Q^2 = 0.54$, RMSECV = 0.18). Across all three seasons, nighttime models exhibited lower cross-validation errors than the corresponding daytime models, with RMSECV ranging from 0.20 to 0.26 °C compared with 0.32 to 0.72 °C during daytime. A detailed summary of the PLS regression models, including component loadings, latent vectors and VIP scores across all seasons, is provided in Section S6 of the Supporting Information.

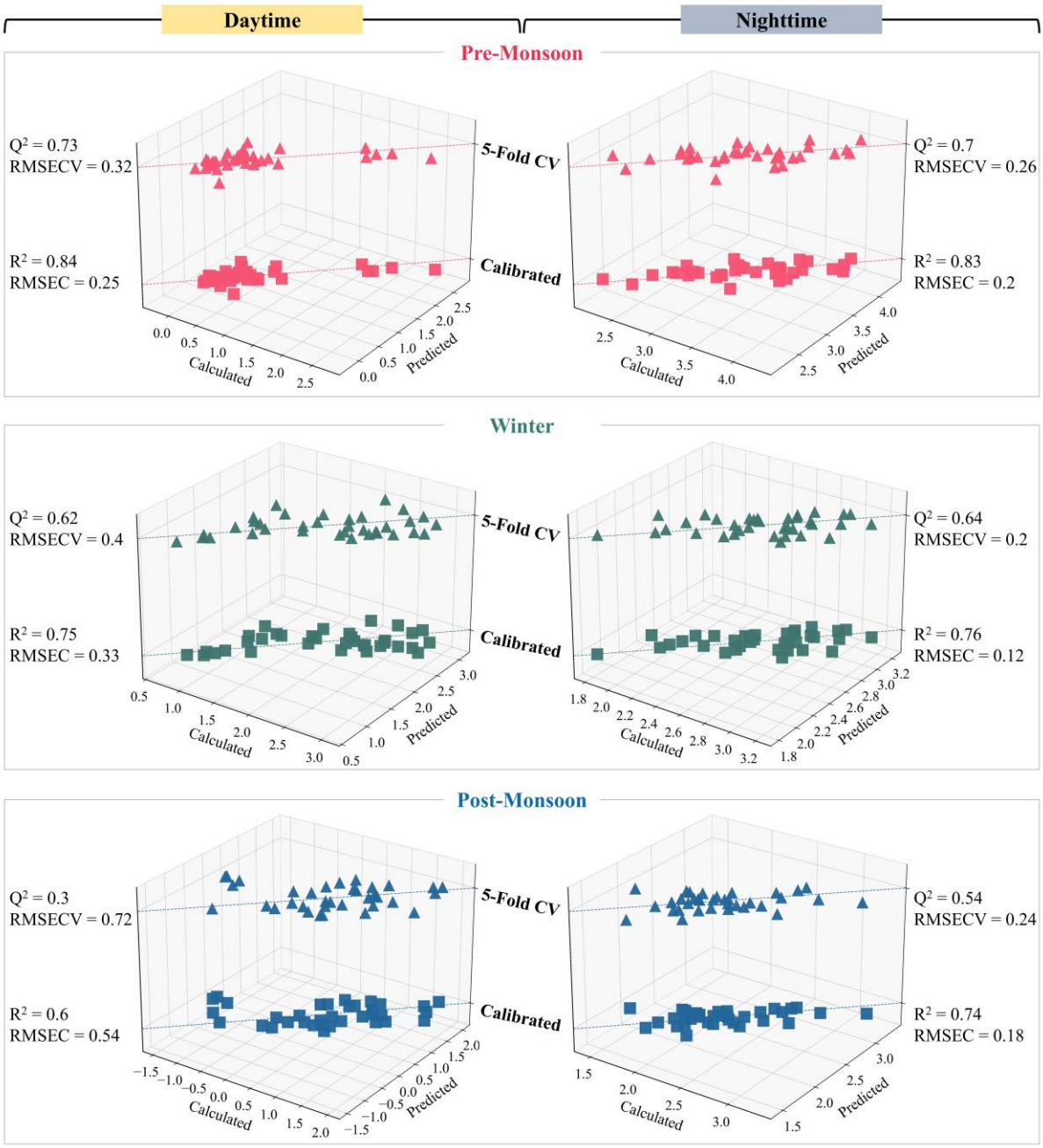


Figure 10: Diagnostic scatter plots of calibrated and 5-fold CV PLS regression models across seasonal regimes for daytime and nighttime

7. Discussion

The multi-decadal SUHI analysis revealed distinct diurnal behaviours across the seven IGP cities, characterized by moderate, variable daytime SUHI alongside consistent, intensified nighttime SUHI. Nighttime mean SUHI exceeded daytime counterparts across all cities and study periods, expanding persistently over the recent pentad (reaching 2.12°C–2.67°C). This nocturnal dominance aligns with broader observations in subtropical and monsoonal urban environments (Derdouri et al., 2021; She et al., 2022), where the daytime storage of sensible heat by dense urban fabrics is released continuously after sunset (Mirza et al., 2026) . The nocturnal persistence of elevated thermal regimes presents pronounced health challenges

across north India, suppressing natural nocturnal physiological cooling and exacerbating thermal discomfort (Shahfahad et al., 2023; Zhu et al., 2021).

The present study highlights the shrinking contrast between urban and rural LSTs, particularly during the pre-monsoon season, where rural daytime LSTs increasingly approach the urban values. This raises a concern that peri-urban warming in Indian cities increasingly blurs the urban–rural boundary, leading to a regional heat island effect instead of urban heat island. Under intense insolation, rural cooling mechanisms largely fail such as post-harvest bare soils, moisture stress, and surface bareness impair daytime evaporative cooling (M. Das et al., 2025; Mallick et al., 2024; Muthiah et al., 2022). Consequently, despite substantial relative increases in rural evapotranspiration (up to +29.70% in Kanpur), its correlation with daytime rural LST is virtually absent ($r = -0.02$), reflecting moisture-limited daytime sensible heating. In contrast, during the night, the RRZ experiences marked cooling. Combined with peripheral BBP expansion across six RRZ (e.g., +20.02% in Varanasi, +11.76% in Patna) and shrinking WBP, rural daytime temperatures approach urban levels, masking localized urban warming within a broader regional heating regime (Kapuganti et al., 2025; Shukla & Jain, 2021). At nighttime, this dynamic reverses as the RRZ transitions into an efficient thermal sink, driving strong nocturnal mean SUHI intensities (2.12°C–2.67°C). High sky-view factors and open canopies facilitate rapid radiational cooling, where rural VP strongly suppresses nighttime rural LST ($r = - 0.60$) and consequently widens nighttime SUHI ($r = 0.52$). On the other hand, rural BBP expansion positively tracks nighttime rural LST ($r = 0.27$), while regional aerosol loading (AOD) correlates positively with nocturnal rural LST ($r = 0.46$) and negatively with nocturnal SUHI ($r = -0.48$), indicating background radiative warming of the rural baseline. This diurnal shift from compromised daytime evaporative cooling to highly efficient nighttime radiative decay demonstrates that SUHI dynamics across the IGP are strongly modulated by the diurnal thermal efficiency of the rural baseline itself.

The empirical relationships identified by the PLS regression models reveal that urban landscape and atmospheric parameters do not function as static, but instead vary across diurnal phases and seasonal transitions. BBP remained the sole persistent positive warming driver across all seasons and diurnal cycles ($p < 0.05$), confirming that replacing natural landcover with impervious materials continuously sustains thermal anomalies through sensible heat storage (Bankoff et al., 2024; Mirza et al., 2021, 2022; Mohammad et al., 2025). Conversely, WBP functioned as a consistent year-round cooling feature ($p < 0.05$), with its highest mitigation efficiency observed during the daytime due to sustained latent heat dissipation (M. Das et al., 2025; Gaber & Özden, 2023). VP exhibited diurnally divergent behaviour. tts daytime cooling is marginal or non-significant, constrained by dry-season moisture deficits and stomatal closure (Zhang et al., 2022), yet it consistently suppressed nighttime SUHI across all seasons ($p < 0.05$ in winter) through unshaded radiative heat loss (She et al., 2022). PD showed an opposing diurnal reversal, switching from a significant negative association during pre-monsoon daytime to a positive nighttime warming driver during winter and post-monsoon. This transition reflects the dual role of compact settlements, which provide daytime mutual building shade but trap sensible heat, lower sky view factors, and release anthropogenic heat at night (Shahfahad et al., 2023; Zhu et al., 2021).

Among the atmospheric parameters, RH switched from a daytime mitigator in pre-monsoon to a strong daytime warming driver in post-monsoon, while consistently acting as a nocturnal cooling agent across all seasons ($p < 0.05$). High moisture content restricts rapid radiative divergence between urban surfaces and the atmosphere at night (Huang et al., 2022; Kim et al., 2025), whereas daytime post-monsoon vapor accumulation suppresses convective venting, trapping sensible heat within humid urban boundary layers (Sismanidis et al., 2022). AOD contributed negatively to daytime SUHI in winter and post-monsoon, yet is reversely acting during nighttime across post-monsoon and winter (Mirza et al., 2023; Nair et al., 2021) . This daytime cooling reflects shortwave solar dimming caused by the dense haze layer (fog blanket), which scatters and absorbs incoming insolation to suppress urban surface heating (Ansari et al., 2025; Tariq et al., 2022). Conversely, during nighttime, elevated aerosol layers absorb and re-emit terrestrial longwave radiation back to the surface, effectively trapping upward thermal flux and sustaining a warmer nocturnal boundary layer that reinforces nighttime SUHI (Kumar et al., 2025; Mostafa et al., 2024). SHF functioned as an effective daytime mitigator during the pre-monsoon but reversed to a significant nocturnal warming enhancer in winter and post-monsoon. While vigorous daytime thermal convection and buoyant plume development assist in shedding urban heat during pre-monsoon extremes (Mohammad et al., 2025), nocturnal sensible heat release from deep urban canyons continues warming the canopy layer, preventing efficient surface cooling (He et al., 2023).

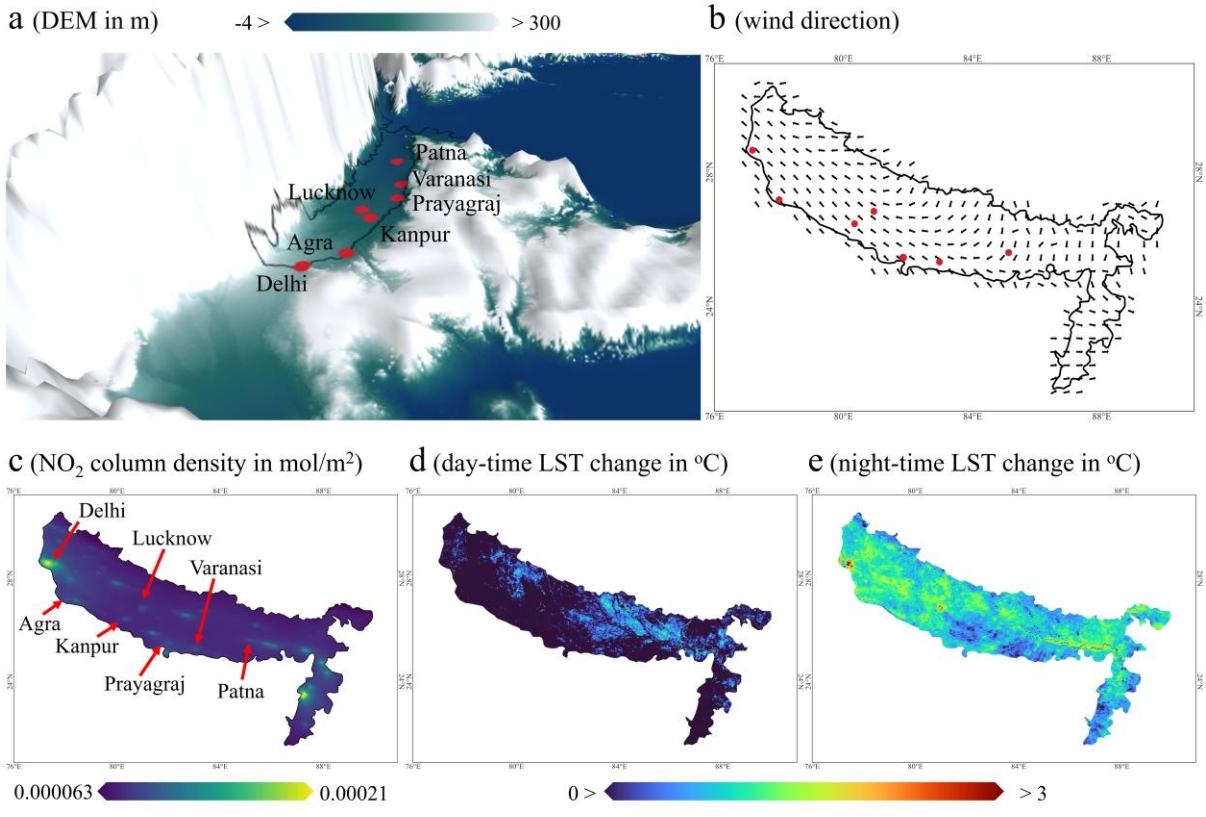


Figure 11: (a) Percentage contribution of atmospheric and landscape parameters; red upward arrows indicating positive contributions that

Figure 11 effectively conceptualizes the IGP as a topographic basin, bounded by the Himalayas to the north and the Vindhyan and Satpura ranges to the south. The DEM over IGP confirms

that all study cities lie within a low-elevation corridor (valley), which fundamentally restricts horizontal and vertical heat dispersion. On an observable level, the synoptic wind vector field (Figure 11b) displays predominantly north westerly winds channelled along this continuous topographical corridor. While these coarse-resolution wind vectors do not represent localized microscale ventilation or complex recirculatory flows but the observable alignment between dominant wind flow, low-lying terrain, and elevated NO_2 plumes (Figure 11c) provides broader geographic context for the regional background environment. This low-lying setting of IGP shares general structural parallels with other major alluvial basins, such as the Nile (Douglas, 1949) and lower Mississippi valleys (McCabe & Wolock, 2019), where river-plain morphology concentrates urban agglomerations within shallow corridors. Because of the unique geography of IGP, cities across the IGP experience a pronounced accumulation of aerosols and the long-term presence of a dense fog blanket over the region (Ansari et al., 2025; Kumar et al., 2025; Miara et al., 2018; Mostafa et al., 2024). The observed spatial correspondence is consistent with a possible contribution of aerosol loading and anthropogenic emissions to nocturnal thermal retention; however, these mechanisms are not directly quantified in the present analysis. Over the IGP, this effect is further magnified due to persistent emissions from traffic, industry, biomass burning, and domestic energy use (Arif et al., 2018; N. Singh et al., 2018).

Limitations and Future Directions:

This study acknowledges following methodological uncertainties and limitations. MODIS LST retrievals (~1 km) carry inherent sensor radiometric uncertainties (~1°C) under elevated aerosol loading and atmospheric haze layers. Some of predictors are derived from ERA5-Land (~11 km) operate at coarser spatial supports compared to high-resolution (10 m) landscape metrics, capturing synoptic background conditions while smoothing localized microclimatic canopy gradients. A fixed 15 km rural reference zone is adopted consistently across the study cities and built-up and water-body pixels are excluded to reduce contamination of the rural baseline. Although the 15 km distance is supported by previous regional assessments, sensitivity of the estimated SUHI to alternative rural-reference distances is not explicitly evaluated and should be examined in future work. Finally, to constrain statistical uncertainty in driver attribution under a moderate sample size, PLS model stability and overfitting are controlled through 5-fold cross-validation and non-parametric bootstrap confidence intervals.

8. Conclusion

This study provides a multi-decadal comparative assessment of SUHI dynamics across seven major cities of the Indo-Gangetic Plains (IGP), using two five-year pentad windows (2000–2004 and 2020–2024) complemented by annual seasonal analysis during 2020–2024. By integrating multi-temporal LST observations, rural reference-zone (RRZ) landscape transitions, synoptic physiographic context, and multivariate attribution using PLS regression, the study provides an updated assessment of the evolving urban–rural thermal regime. Across all evaluated cities, nighttime SUHI consistently exceeded daytime SUHI in mean intensity during both pentad periods, with nighttime warming remaining spatially widespread across the

urban areas. A key finding is the narrowing of the urban–rural thermal contrast, particularly during the pre-monsoon season, when rural daytime LST increasingly approaches urban values. This pattern is associated with changes in the rural reference environment, including moisture deficits, post-harvest bare soils, and peripheral built-up expansion, which may weaken daytime rural evaporative cooling. The results further indicate that SUHI dynamics are governed by seasonally and diurnally varying interactions between urban landscape and atmospheric conditions. Built-up and bare-surface proportion (BBP) emerged as a persistent positive predictor of SUHI, whereas water-body proportion (WBP) showed a consistent mitigating association, particularly during daytime. Vegetation proportion (VP) exhibited predominantly negative nighttime associations but weaker and more variable daytime relationships across seasons. Population density and atmospheric variables, including relative humidity, wind speed, sensible heat flux, and aerosol optical depth, also exhibited season- and diurnally dependent associations rather than uniformly consistent effects. The observed nighttime thermal persistence occurs in the context of the topographically constrained IGP basin, regional synoptic flow patterns, and elevated aerosol loading; these factors provide physiographic and atmospheric context for the observed thermal regime, although their individual causal contributions are not directly quantified in the present study. Overall, the findings indicate that urban heat mitigation in the IGP cannot be considered solely within municipal boundaries. Effective regional heat-resilience strategies should account for peri-urban landscape transformation, expansion of built and bare surfaces, preservation of blue infrastructure, maintenance of vegetation, and changing atmospheric conditions across the urban–rural continuum.

Author contributions

Shahid Mirza: Conceptualization, Data curation, Formal analysis, Investigation, Methodology, Software, Visualization, Writing – original draft.

Rohini Lakshman Bhawar: Formal analysis, Methodology, Validation, Writing – review and editing.

Sunil R. Patil: Conceptualization, Formal analysis, Methodology, Software, Supervision, Writing – review and editing.

Data availability

All the data used/generated during this study will be made available upon reasonable request.

Declarations

Ethics approval: Not applicable.

Consent to publish: Not applicable

Consent to publish: Not applicable.

Competing interests: The authors declare no competing interests.

Funding Declaration: There is no funding provided for this research work.

Clinical trial number: Not applicable.

References

Abdi, H., & Williams, L. J. (2010). Principal component analysis. *Wiley Interdisciplinary Reviews: Computational Statistics*, *2*(4), 433–459. https://doi.org/10.1002/WICS.101

Alduchov, O. A., Eskridge, R. E., Alduchov, O. A., Eskridge, R. E., Alduchov, A., O., Eskridge, & E., R. (1996). Improved Magnus Form Approximation of Saturation Vapor Pressure. *JApMe*, *35*(4), 601–609. https://doi.org/10.1175/1520-0450(1996)035

Ansari, N., Kumari, P., Kumar, R., Kumar, P., Shamshad, A., Hossain, S., Sharma, A., Singh, Y., Kumari, M., Mishra, V. N., Rukhsana, & Javed, A. (2025). Seasonal patterns of air pollution in Delhi: interplay between meteorological conditions and emission sources. *Environmental Geochemistry and Health 2025 47:5*, *47*(5), 175-. https://doi.org/10.1007/S10653-025-02474-0

Arif, M., Kumar, R., Kumar, R., Zusman, E., Singh, R. P., & Gupta, A. (2018). Assessment of Indoor & Outdoor Black Carbon emissions in rural areas of Indo-Gangetic Plain: seasonal characteristics, source apportionment and radiative forcing. *Atmospheric Environment*, *191*, 227–240. https://doi.org/10.1016/J.ATMOSENV.2018.07.057

Bankoff, G., Chakravarty, S., & Jordan, S. (2024). The warming city: the increasing risk of summer fires in Delhi. *Disasters*, *48*(1), e12601. https://doi.org/10.1111/DISA.12601;REQUESTEDJOURNAL:JOURNAL:14677717;WGROUP:STRING:PUBLICATION

Bhaga, T. D., Dube, T., Shekede, M. D., & Shoko, C. (2023). Investigating the effectiveness of Landsat-8 OLI and Sentinel-2 MSI satellite data in monitoring the effects of drought on surface water resources in the Western Cape Province, South Africa. *Remote Sensing Applications: Society and Environment*, *32*, 101037. https://doi.org/10.1016/J.RSASE.2023.101037

Bhanage, V., Kulkarni, S., Sharma, R., Lee, H. S., & Gedam, S. (2023). Enumerating and Modelling the Seasonal alterations of Surface Urban Heat and Cool Island: A Case Study over Indian Cities. *Urban Science 2023, Vol. 7, Page 38*, *7*(2), 38. https://doi.org/10.3390/URBANSCI7020038

Brown, C. F., Brumby, S. P., Guzder-Williams, B., Birch, T., Hyde, S. B., Mazzariello, J., Czerwinski, W., Pasquarella, V. J., Haertel, R., Ilyushchenko, S., Schwehr, K., Weisse, M., Stolle, F., Hanson, C., Guinan, O., Moore, R., & Tait, A. M. (2022). Dynamic World, Near real-time global 10 m land use land cover mapping. *Scientific Data*, *9*(1). https://doi.org/10.1038/S41597-022-01307-4

Chatterjee, S., Das, M., Rai, H., Singh, D., Preeti, K., & Pandey, V. (2022). Gangetic Plains of India: High on the Water and Air Pollution Map. *Forest Dynamics and Conservation:*

Science, Innovations and Policies, 83–106. https://doi.org/10.1007/978-981-19-0071-6_4

Clinton, N., & Gong, P. (2013). MODIS detected surface urban heat islands and sinks: Global locations and controls. *Remote Sensing of Environment*, *134*, 294–304. https://doi.org/10.1016/J.RSE.2013.03.008

Coombe, Penny., & Fung, Y. Tung. (2022). *Approaches to Disruptions and Interactions in Archaeology : Proceedings of the Graduate Archaeology at Oxford Annual Conferences in 2017-2019*. 1–132.

Dagestani, A. A., Tariq, S., Khan, M., Kamal, M., & Rehman, M. ur. (2024). Assessment of nighttime air quality over an urban location in Indo-Gangetic plain using remote sensing observations. *Atmospheric Pollution Research*, *15*(2), 101982. https://doi.org/10.1016/J.APR.2023.101982

Dangayach, R., & Pandey, A. K. (2024). Unraveling the Complex Relationships Between Aerosol Optical Depth and Temperature: A Review. *Aerosol Optical Depth and Precipitation: Measuring Particle Concentration, Health Risks and Environmental Impacts*, 1–18. https://doi.org/10.1007/978-3-031-55836-8_1

Das, A., Saha, P., Dasgupta, R., Inacio, M., Das, M., & Pereira, P. (2024). How Do the Dynamics of Urbanization Affect the Thermal Environment? A Case from an Urban Agglomeration in Lower Gangetic Plain (India). *Sustainability (Switzerland)*, *16*(3), 1147. https://doi.org/10.3390/SU16031147/S1

Das, M., Das, A., Das, S., & Pereira, P. (2025). Assessing urban heat island dynamics in India: the role of socio-economic and environmental factors. *Environment, Development and Sustainability*, 1–23. https://doi.org/10.1007/S10668-025-06161-Z/METRICS

Debbage, N., & Shepherd, J. M. (2015). The urban heat island effect and city contiguity. *Computers, Environment and Urban Systems*, *54*, 181–194. https://doi.org/10.1016/J.COMPENVURBSYS.2015.08.002

Derdouri, A., Wang, R., Murayama, Y., & Osaragi, T. (2021). Understanding the links between lulc changes and suhi in cities: Insights from two-decadal studies (2001–2020). *Remote Sensing*, *13*(18), 3654. https://doi.org/10.3390/RS13183654/S1

Ding, L., Xiao, X., & Wang, H. (2025). Temporal and spatial variations of urban surface temperature and correlation study of influencing factors. *Scientific Reports 2025 15:1*, *15*(1), 914-. https://doi.org/10.1038/s41598-025-85146-4

Douglas, C. (1949). *Geography and Politics in the Nile Valley on JSTOR* (Vol. 3). Middle East Institute. https://www.jstor.org/stable/4322085

Du, R., Liu, C. H., Li, X., & Lin, C. Y. (2024). Interaction among local flows, UHI, coastal winds, and complex terrain: Effect on urban-scale temperature and building energy consumption during heatwaves. *Energy and Buildings*, *303*, 113763. https://doi.org/10.1016/J.ENBUILD.2023.113763

Fadhil, M., Hamoodi, M. N., & Ziboon, A. R. T. (2023). Mitigating urban heat island effects in urban environments: strategies and tools. *IOP Conference Series: Earth and*

Environmental Science, *1129*(1), 012025. https://doi.org/10.1088/1755-1315/1129/1/012025

Gaber, M., & Özden, Ö. (2023). Urban Growth and Its Environmental Impacts: Case of the Nile River, Egypt. *Journal of Urban Culture Research*, *26*, 237–244. https://doi.org/10.14456/JUCR.2023.14

Gaughan, A. E., Stevens, F. R., Linard, C., Jia, P., & Tatem, A. J. (2013). High Resolution Population Distribution Maps for Southeast Asia in 2010 and 2015. *PLOS ONE*, *8*(2), e55882. https://doi.org/10.1371/JOURNAL.PONE.0055882

Geetha B. Nambissan. (2021). *The Changing Urban and Education in Delhi: Privilege and Exclusion in a Megacity MaxWeber Stiftung*.

Gupta, L., Bansal, M., Nandi, P., Habib, G., & Sunder Raman, R. (2023). Source apportionment and potential source regions of size-resolved particulate matter at a heavily polluted industrial city in the Indo-Gangetic Plain. *Atmospheric Environment*, *298*, 119614. https://doi.org/10.1016/J.ATMOSENV.2023.119614

He, X., Gao, W., Wang, R., & Yan, D. (2023). Study on outdoor thermal comfort of factory areas during winter in hot summer and cold winter zone of China. *Building and Environment*, *228*, 109883. https://doi.org/10.1016/J.BUILDENV.2022.109883

Huang, J., Lin, C., Li, Y., & Huang, B. (2022). Effects of humidity, aerosol, and cloud on subambient radiative cooling. *International Journal of Heat and Mass Transfer*, *186*, 122438. https://doi.org/10.1016/J.IJHEATMASSTRANSFER.2021.122438

Humbal, A., Chaudhary, N., & Pathak, B. (2023). *Urbanization Trends, Climate Change, and Environmental Sustainability*. 151–166. https://doi.org/10.1007/978-981-19-7618-6_9

Islam, S., Karipot, A., Bhawar, R., Sinha, P., Kedia, S., & Khare, M. (2024). Urban heat island effect in India: a review of current status, impact and mitigation strategies. *Discover Cities 2024 1:1*, *1*(1), 1–28. https://doi.org/10.1007/S44327-024-00033-3

Jha, R., Mondal, A., Devanand, A., Roxy, M. K., & Ghosh, S. (2022). Limited influence of irrigation on pre-monsoon heat stress in the Indo-Gangetic Plain. *Nature Communications*, *13*(1), 1–10. https://doi.org/10.1038/S41467-022-31962-5;TECHMETA

Kapuganti, D. K., Tiwari, K. C., & Areendran, G. (2025). Assessing land surface temperature dynamics and urban heat island effects in Delhi: a multi-temporal analysis and future projections. *Environmental Monitoring and Assessment 2025 197:10*, *197*(10), 1094-. https://doi.org/10.1007/S10661-025-14390-Y

Kim, Y., Yoo, C., & Im, J. (2025). Nighttime satellite land surface temperature for urban applications: achievements, challenges, and future prospects. *GIScience and Remote Sensing*, *62*(1). https://doi.org/10.1080/15481603.2025.2527990;PAGE:STRING:ARTICLE/CHAPTER

Kumar, R., Meech, S., Yadav, P. P., Cheng, W. Y. Y., Ghude, S. D., Alessandrini, S., Jat, R., & Govardhan, G. (2025). Will assimilating VIIRS AOD data improve New Delhi's air

766 pollution forecasts as much as assimilating MODIS AOD? *Atmospheric Environment*,
767 *361*, 121526. https://doi.org/10.1016/J.ATMOSENV.2025.121526

768 Lawrence, M. G. (2004). The Relationship between Relative Humidity and the Dewpoint
769 Temperature in Moist Air A Simple Conversion and Applications. *AMERICAN*
770 *METEOROLOGICAL SOCIETY*. https://doi.org/10.1175/BAMS-86-2-225

771 Liao, S., Cai, H., Tian, P., Zhang, B., & Li, Y. (2022). Combined impacts of the abnormal and
772 urban heat island effect in Guiyang, a typical Karst Mountain City in China. *Urban*
773 *Climate*, *41*, 101014. https://doi.org/10.1016/J.UCLIM.2021.101014

774 Lyapustin, A., & Wang, Y. (2022). *MODIS/Terra+Aqua Land Aerosol Optical Depth Daily*
775 *L2G Global 1km SIN Grid V061 | NASA Earthdata*.
776 https://www.earthdata.nasa.gov/data/catalog/lpcloud-mcd19a2-061

777 Mallick, S. K., Sahu, N., Das, P., Maity, B., Varun, A., Kumar, A., Keswarwani, R., Saini, A.,
778 & Rudra, S. (2024). Impact of urban growth in Delhi and It's Peri-urban environment on
779 urban heat exposure. *Urban Climate*, *56*, 102010.
780 https://doi.org/10.1016/J.UCLIM.2024.102010

781 McCabe, G. J., & Wolock, D. M. (2019). Hydroclimatology of the Mississippi River Basin.
782 *Journal of the American Water Resources Association*, *55*(4), 1053–1064.
783 https://doi.org/10.1111/1752-1688.12749;PAGEGROUP:STRING:PUBLICATION

784 Mehak Rattan, G. S. S. and S. K. S. (2021). HISTORY OF LAND USE IN THE INDO
785 GANGETIC PLAINS, INDIA AND ITS IMPACT ON POPULATION: A REVIEW .
786 *Plant Archives*, *21*, 532–537.
787 https://doi.org/10.51470/PLANTARCHIVES.2021.v21.S1.082

788 Miara, A., Vörösmarty, C. J., Macknick, J. E., Tidwell, V. C., Fekete, B., Corsi, F., &
789 Newmark, R. (2018). Thermal pollution impacts on rivers and power supply in the
790 Mississippi River watershed. *Environmental Research Letters*, *13*(3), 034033.
791 https://doi.org/10.1088/1748-9326/AAAC85

792 Mirza, S., Bhawar, R. L., & Patil, S. R. (2026). Spatiotemporal trends of land surface
793 temperature and surface urban heat island intensification across India. *Environmental*
794 *Monitoring and Assessment 2026 198:4*, *198*(4), 324-. https://doi.org/10.1007/S10661-
795 026-15153-Z

796 Mirza, S., Niwalkar, A., Anjum, S., Bherwani, H., Singh, A., & Kumar, R. (2021).
797 INTEGRATED ASSESSMENT OF URBAN MICROCLIMATE PARAMETERS
798 USING OPEN FOAM. *Vidyabharati International Interdisciplinary Research Journal*
799 *(Special Issue)*, 118–130.

800 Mirza, S., Niwalkar, A., Anjum, S., Bherwani, H., Singh, A., & Kumar, R. (2022). Studying
801 impact of infrastructure development on urban microclimate: Integrated multiparameter
802 analysis using OpenFOAM. *Energy Nexus*, *6*.
803 https://doi.org/10.1016/j.nexus.2022.100060

804 Mirza, S., Niwalkar, A., Gupta, A., Gautam, S., Anshul, A., Bherwani, H., Biniwale, R., &
805 Kumar, R. (2023). Is safe distance enough to prevent COVID-19? Dispersion and

tracking of aerosols in various artificial ventilation conditions using OpenFOAM. *Gondwana Research*, *114*, 40–54. https://doi.org/10.1016/j.gr.2022.03.013

Mishra, M. K., & Mathew, A. (2022). Investigating the spatio-temporal correlation between urban heat island and atmospheric pollution island interaction over Delhi, India using geospatial techniques. *Arabian Journal of Geosciences 2022 15:20*, *15*(20), 1–27. https://doi.org/10.1007/S12517-022-10854-4

Mohammad, S., Mohd. Nazish, K., Ganiyeva, S., Odinaevich, A. B., & Ali, D. (2025). *Estimating extreme heat event over New Delhi Region, India using Satellite Data*. *17*(2), 802–809. https://www.researchgate.net/profile/Mohammad-Suhail-2/publication/392892472_Estimating_extreme_heat_event_over_New_Delhi_Region_India_using_Satellite_Data/links/68567832e8fa0f5c28258fc9/Estimating-extreme-heat-event-over-New-Delhi-Region-India-using-Satellite-Data.pdf

Mostafa, A. N., Alfaro, S. C., Robaa, S. M., Zakey, A. S., & Abdel Wahab, M. M. (2024). Heatwaves and Their Impact on Air Quality in Greater Cairo, Egypt. *Atmosphere 2024, Vol. 15, 15*(6). https://doi.org/10.3390/ATMOS15060637

Muthiah, K., Mathivanan, M., & Duraisekaran, E. (2022). Dynamics of urban sprawl on the peri-urban landscape and its relationship with urban heat island in Chennai Metropolitan Area, India. *Arabian Journal of Geosciences 2022 15:23*, *15*(23), 1694-. https://doi.org/10.1007/S12517-022-10959-W

Nair, M., Bherwani, H., Mirza, S., Anjum, S., & Kumar, R. (2021). Valuing burden of premature mortality attributable to air pollution in major million-plus non-attainment cities of India. *Scientific Reports*, *11*(1), 1–15. https://doi.org/10.1038/S41598-021-02232-Z;SUBJMETA

Nayak, S., Vinod, A., & Prasad, A. K. (2023). Spatial Characteristics and Temporal Trend of Urban Heat Island Effect over Major Cities in India Using Long-Term Space-Based MODIS Land Surface Temperature Observations (2000–2023). *Applied Sciences 2023, Vol. 13, Page 13323*, *13*(24), 13323. https://doi.org/10.3390/APP132413323

Nikkath, S. N., & Selvi, S. T. (2024). Anthropogenic Influence on Aerosol Optical Depth. *Aerosol Optical Depth and Precipitation: Measuring Particle Concentration, Health Risks and Environmental Impacts*, 245–263. https://doi.org/10.1007/978-3-031-55836-8_15

Oğur, A. A. (2023). Uneven resilience of urban and rural areas to heatwaves. *Journal of Design for Resilience in Architecture and Planning*, *4*((Special Issue)), 78–94. https://doi.org/10.47818/DRArch.2023.v4si111

Oh, S. G., Han, J. Y., Min, S. K., & Son, S. W. (2023). Impact of urban heat island on daily and sub-daily monsoon rainfall variabilities in East Asian megacities. *Climate Dynamics*, *61*(1–2), 19–32. https://doi.org/10.1007/S00382-022-06556-Y/METRICS

Pedregosa, F., Varoquaux, G., Gramfort, A., Michel, V., Thirion, B., Grisel, O., Blondel, M., Müller, A., Nothman, J., Louppe, G., Prettenhofer, P., Weiss, R., Dubourg, V., Vanderplas, J., Passos, A., Cournapeau, D., Brucher, M., Perrot, M., & Duchesnay, É. (2018). *Scikit-learn: Machine Learning in Python*. http://arxiv.org/abs/1201.0490

Peng, S., Piao, S., Ciais, P., Friedlingstein, P., Ottle, C., Bréon, F. M., Nan, H., Zhou, L., & Myneni, R. B. (2012). Surface urban heat island across 419 global big cities. *Environmental Science & Technology*, *46*(2), 696–703. https://doi.org/10.1021/ES2030438

Ramachandran, S., & Rupakheti, M. (2022). Trends in the types and absorption characteristics of ambient aerosols over the Indo-Gangetic Plain and North China Plain in last two decades. *Science of The Total Environment*, *831*, 154867. https://doi.org/10.1016/J.SCITOTENV.2022.154867

Rao, P., Gupta, K., Roy, A., & Balan, R. (2021). Spatio-temporal analysis of land surface temperature for identification of heat wave risk and vulnerability hotspots in Indo-Gangetic Plains of India. *Theoretical and Applied Climatology*, *146*(1–2), 567–582. https://doi.org/10.1007/S00704-021-03756-0/METRICS

Rath, S. S., Panda, J., & Sarkar, A. (2022). Distinct urban land cover response to meteorology in WRF simulated pre-monsoon thunderstorms over the tropical city of Kolkata. *Meteorology and Atmospheric Physics*, *134*(4), 1–23. https://doi.org/10.1007/S00703-022-00916-3/METRICS

Roy, P. S., Ramachandran, R. M., Paul, O., Thakur, P. K., Ravan, S., Behera, M. D., Sarangi, C., & Kanawade, V. P. (2022). Anthropogenic Land Use and Land Cover Changes—A Review on Its Environmental Consequences and Climate Change. In *Journal of the Indian Society of Remote Sensing* (Vol. 50, Number 8, pp. 1615–1640). Springer. https://doi.org/10.1007/s12524-022-01569-w

Running, S., Mu, Q., Zhao, M., Moreno, A., Running, Steve, Mu, Qiaozhen, Zhao, Maosheng, Moreno, & Alvaro. (2021). MODIS/Terra Net Evapotranspiration Gap-Filled 8-Day L4 Global 500m SIN Grid V061. *Lp*, 384. https://doi.org/10.5067/MODIS/MOD16A2GF.061

Sabater, M. (2019). ERA5-land monthly averaged data from 1981 to present, Copernicus Climate Change Service (C3S) Climate Data Store (CDS). *Earth Syst. Sci.* https://cir.nii.ac.jp/crid/1370869855589506946

Shahfahad, Bindajam, A. A., Naikoo, M. W., Talukdar, S., Asif, Mallick, J., & Rahman, A. (2023). Analysing diurnal temperature range and extreme temperature events over Delhi and Mumbai mega cities. *Natural Hazards 2023 120:10*, *120*(10), 9267–9295. https://doi.org/10.1007/S11069-023-06077-9

Sharma, P., Peshin, S. K., Soni, V. K., Singh, S., Beig, G., & Ghosh, C. (2022). Seasonal dynamics of particulate matter pollution and its dispersion in the city of Delhi, India. *Meteorology and Atmospheric Physics*, *134*(2), 1–18. https://doi.org/10.1007/S00703-021-00852-8/METRICS

She, Y., Liu, Z., Zhan, W., Lai, J., & Huang, F. (2022). Strong regulation of daily variations in nighttime surface urban heat islands by meteorological variables across global cities. *Environmental Research Letters*, *17*(1), 014049. https://doi.org/10.1088/1748-9326/AC4630

Shukla, A., & Jain, K. (2021). Analyzing the impact of changing landscape pattern and dynamics on land surface temperature in Lucknow city, India. *Urban Forestry & Urban Greening*, *58*, 126877. https://doi.org/10.1016/J.UFUG.2020.126877

Si, M., Li, Z. L., Nerry, F., Tang, B. H., Leng, P., Wu, H., Zhang, X., & Shang, G. (2022). Spatiotemporal pattern and long-term trend of global surface urban heat islands characterized by dynamic urban-extent method and MODIS data. *ISPRS Journal of Photogrammetry and Remote Sensing*, *183*, 321–335. https://doi.org/10.1016/J.ISPRSJPRS.2021.11.017

Singh, N., Banerjee, T., Raju, M. P., Deboudt, K., Sorek-Hamer, M., Singh, R. S., & Mall, R. K. (2018). Aerosol chemistry, transport, and climatic implications during extreme biomass burning emissions over the Indo-Gangetic Plain. *Atmospheric Chemistry and Physics*, *18*(19), 14197–14215. https://doi.org/10.5194/ACP-18-14197-2018

Singh, P., Verma, P., Chaudhuri, A. S., Singh, V. K., & Rai, P. K. (2024). Evaluating the relationship between Urban Heat Island and temporal change in land use, NDVI and NDBI: a case study of Bhopal city, India. *International Journal of Environmental Science and Technology*, *21*(3), 3061–3072. https://doi.org/10.1007/S13762-023-05141-Y/METRICS

Singh, R., Rakesh, V., & Varma, A. K. (2023). Association of winter vegetation activity across the indo-gangetic plain with the subsequent Indian summer monsoon rainfall. *Climate Dynamics*, *60*(7–8), 2245–2259. https://doi.org/10.1007/S00382-022-06426-7/METRICS

Singh, T., Ravindra, K., Beig, G., & Mor, S. (2021). Influence of agricultural activities on atmospheric pollution during post-monsoon harvesting seasons at a rural location of Indo-Gangetic Plain. *Science of The Total Environment*, *796*, 148903. https://doi.org/10.1016/J.SCITOTENV.2021.148903

Sismanidis, P., Bechtel, B., Perry, M., & Ghent, D. (2022). The Seasonality of Surface Urban Heat Islands across Climates. *Remote Sensing 2022, Vol. 14, Page 2318*, *14*(10), 2318. https://doi.org/10.3390/RS14102318

Stewart, I. D. ., & Mills, G. M. . (2021). *The urban heat island : a guidebook*.

Taloor, A. K., Drinder Singh Manhas, & Chandra Kothyari, G. (2021). Retrieval of land surface temperature, normalized difference moisture index, normalized difference water index of the Ravi basin using Landsat data. *Applied Computing and Geosciences*, *9*, 100051. https://doi.org/10.1016/J.ACAGS.2020.100051

Taloor, A. K., Parsad, G., Jabeen, S. F., Sharma, M., Choudhary, R., & Kumar, A. (2024). Analytical study of land surface temperature for evaluation of UHI and UHS in the city of Chandigarh India. *Remote Sensing Applications: Society and Environment*, *35*, 101206. https://doi.org/10.1016/J.RSASE.2024.101206

Tariq, S., Qayyum, F., Ul-Haq, Z., & Mehmood, U. (2022). Long-term spatiotemporal trends in aerosol optical depth and its relationship with enhanced vegetation index and meteorological parameters over South Asia. *Environmental Science and Pollution*

Research 2021 29:20, *29*(20), 30638–30655. https://doi.org/10.1007/S11356-021-17887-4

Wan, Z., Hook, S., Processes, G. H.-N. E. L., & 2015, undefined. (2015). MYD11A1 MODIS/aqua land surface temperature/emissivity daily L3 global 1km SIN grid V006. *Ui.Adsabs.Harvard.Edu*. https://doi.org/10.5067/MODIS/MYD11A1.006

Wang, Z., Xue, L., Liu, J., Ding, K., Lou, S., Ding, A., Wang, J., & Huang, X. (2022). Roles of Atmospheric Aerosols in Extreme Meteorological Events: a Systematic Review. *Current Pollution Reports*, *8*(2), 177–188. https://doi.org/10.1007/S40726-022-00216-9/METRICS

Wold, S., Sjöström, M., & Eriksson, L. (2001). PLS-regression: a basic tool of chemometrics. *Chemometrics and Intelligent Laboratory Systems*, *58*(2), 109–130. https://doi.org/10.1016/S0169-7439(01)00155-1

WorldPop. (2026). *WorldPop Global Project Population Data: Estimated Residential Population per 100x100m Grid Square | Earth Engine Data Catalog | Google for Developers*. https://developers.google.com/earth-engine/datasets/catalog/WorldPop_GP_100m_pop#citations

Wu, X., & Zhang, Y. (2023). Coupling analysis of ecological environment evaluation and urbanization using projection pursuit model in Xi'an, China. *Ecological Indicators*, *156*, 111078. https://doi.org/10.1016/J.ECOLIND.2023.111078

Yang, M., Ren, C., Wang, H., Wang, J., Feng, Z., Kumar, P., Haghighat, F., & Cao, S.-J. (2024). Mitigating urban heat island through neighboring rural land cover. *Nature Cities 2024 1:8*, *1*(8), 522–532. https://doi.org/10.1038/s44284-024-00091-z

Yao, R., Wang, L., Huang, X., Gong, W., & Xia, X. (2019). Greening in Rural Areas Increases the Surface Urban Heat Island Intensity. *Geophysical Research Letters*, *46*(4), 2204–2212. https://doi.org/10.1029/2018GL081816;WGROUP:STRING:PUBLICATION

Zeynali, R., Mandanici, E., & Bitelli, G. (2026). Urban Heat Island: Assessing the Influence of Urban Morphology on Air and Surface Temperatures. *Sustainability 2026, Vol. 18, Page 1695*, *18*(3), 1695. https://doi.org/10.3390/SU18031695

Zhang, Y., Piao, S., Sun, Y., Rogers, B. M., Li, X., Lian, X., Liu, Z., Chen, A., & Peñuelas, J. (2022). Future reversal of warming-enhanced vegetation productivity in the Northern Hemisphere. *Nature Climate Change 2022 12:6*, *12*(6), 581–586. https://doi.org/10.1038/s41558-022-01374-w

Zheng, S., He, C., Guldmann, J. M., Xu, H., & Liu, X. (2023). Heat Mitigation Benefits of Urban Trees: A Review of Mechanisms, Modeling, Validation and Simulation. *Forests 2023, Vol. 14, Page 2280*, *14*(12), 2280. https://doi.org/10.3390/F14122280

Zhu, J., Wang, S., & Fischer, E. M. (2021). Increased occurrence of day–night hot extremes in a warming climate. *Climate Dynamics 2021 59:5*, *59*(5), 1297–1307. https://doi.org/10.1007/S00382-021-06038-7

Supplementary Files

This is a list of supplementary files associated with this preprint. Click to download.

- SupportingInformation.docx